A non-canonical lipid droplet metabolism regulates the conversion of alpha-Synuclein to proteolytic resistant forms in neurons of a *Drosophila* model of Parkinson disease

Victor Girard[1], Florence Jollivet[1], Oskar Knittelfelder[2], Jean-Noel Arsac[3], Gilles Chatelain[1], Daan M. Van den Brink[1,4], Thierry Baron[3], Andrej Shevchenko[2], Nathalie Davoust[1,*], Bertrand Mollereau[1,*]

[1] Laboratory of Biology and Modelling of the Cell, UMR5239 CNRS/ENS de Lyon, INSERM U1210, UMS 3444 Biosciences Lyon Gerland, University of Lyon, F-69342, Lyon, France.
[2] Max-Planck-Institute of Molecular Cell Biology and Genetics, Pfotenhauerstraße 108, 01307 Dresden, Germany.
[3] Neurodegenerative Disease Unit; French Agency for Food, Environmental and Occupational Health & Safety (Anses) Laboratory of Lyon, Université de Lyon, Lyon, France.
[4] Plant Systems Physiology, Institute for Water and Wetland Research, Radboud University, PO Box 9010, 6500 GL Nijmegen, The Netherlands.

*Co-senior and co-corresponding authors: nathalie.davoust-nataf@ens-lyon.fr and bertrand.mollereau@ens-lyon.fr

Abstract

Parkinson's disease (PD) is a neurodegenerative disorder characterized by alpha-synuclein (αSyn) aggregation and associated with abnormalities in lipid metabolism. The accumulation of lipids in cytoplasmic organelles called lipid droplets (LDs) was observed in cellular models of PD. To investigate the pathophysiological consequences of interactions between αSyn and proteins that regulate the homeostasis of LDs, we used a transgenic *Drosophila* model of PD, in which human αSyn is specifically expressed in photoreceptor neurons. We first found that overexpression of the LD-coating proteins perilipin 1 or 2 (dPlin1/2), which limit the access of lipases to LDs, markedly increased triacylglyclerol (TG) loaded LDs in neurons. However, dPlin-induced-LDs in neurons are independent of lipid anabolic (diacylglycerol acyltransferase 1/Midway, fatty acid transport protein/dFatp) and catabolic (lipase Brummer) enzymes, indicating that non-canonical mechanisms regulate neuronal LD homeostasis. Interestingly, the accumulation of LDs induced by several distinct LD proteins (dPlin1, dPlin2, CG7900 or Klarsicht$^{LD\text{-}BD}$) was synergistically amplified by the co-expression of αSyn, which was found at the surface of LDs both in photoreceptors neurons of *Drosophila* and in human neuroblastoma cells. Finally, the accumulation of LDs increased the resistance of αSyn to proteolytic digestion, a phenomenon associated with αSyn aggregation in human neurons. We thus propose that αSyn cooperates with LD proteins to inhibit lipolysis and that binding of αSyn to LDs contributes to the pathogenic misfolding and aggregation of αSyn in neurons.

Introduction

Lipids play crucial roles in many essential cellular functions, including membrane formation, energy production, intracellular and intercellular signal transduction, and regulation of cell death. Fatty acids (FAs) taken up into or synthesized within cells are stored in discrete organelles known as lipid droplets (LDs), which consist of a core of neutral lipids predominantly triacylglycerols (TGs) and sterol esters, surrounded by a monolayer of phospholipids containing numerous LD proteins (Olzmann and Carvalho, 2019). Maintenance of LD homeostasis in adipose tissue and in the central nervous system, among other tissues, has emerged as a central process for organismal health, and its dysregulation contributes to many human diseases, such as obesity, atherosclerosis, fatty liver disease, and neurodegenerative disorders such as Parkinson's disease (PD) (Fanning et al., 2020; Farmer et al., 2020; Krahmer et al., 2013; Pennetta and Welte, 2018).

The mechanisms by which fat is stored and remobilized in LDs are dependent of evolutionary conserved canonical anabolic and catabolic enzymes (Heier and Kühnlein, 2018). LD biogenesis is initiated at the endoplasmic reticulum membrane, where lipogenesis enzymes, such as *Drosophila* diacylglycerol acyltransferase 1 (DGAT1), encoded by the *midway (Mdy)* gene, catalyze the rate limiting step of TG synthesis (Beller et al., 2010; Buszczak et al., 2002). Also, Fatty acid transport protein 1 (dFatp in *Drosophila*), which functions in a complex with diacylglycerol acyltransferase 2 (DGAT2), promotes LD expansion in *C. elegans*, *Drosophila* and mammalian cells (Dourlen et al., 2015; Van Den Brink et al., 2018; Xu et al., 2012). Several other components have also been identified, such as Seipin proteins which form a ring-link structure that facilitate the flow of TGs within LDs (Jackson, 2019; Salo et al., 2019). In contrast, lipolysis is catalysed by lipases, such as the central and evolutionarily conserved TG lipase Brummer in the fly (Bmm also called dATGL), ortholog of mammalian adipose triglyceride lipase (ATGL) (Grönke et al., 2005).

Lipase activity is controlled by a family of LD proteins called perilipins (PLINs) that play different roles in LD homeostasis, including maintaining LD integrity, limiting basal lipolysis, and interacting with mitochondria (Kimmel and Sztalryd, 2016). The human genome encodes five PLIN proteins, PLIN1–5 (Itabe et al., 2017; Kimmel and Sztalryd, 2016; Sztalryd and Brasaemle, 2017), whereas the *Drosophila* genome encodes two PLINs, Lsd-1 and Lsd-2 (hereafter named dPlin1 and dPlin2) that play distinct roles in LD homeostasis (Heier and Kühnlein, 2018). dPlin2 is indeed considered as the guardian of LDs by shielding LD away from

lipases, while dPlin1 by interacting directly with lipases can either stimulate or inhibit lipolysis (Beller et al., 2006, 2010; Bi et al., 2012; Grönke et al., 2003). *dPlin1* expression, like that of human *PLIN1*, is mainly restricted to adipose tissue, but it was also found expressed in *Drosophila* wing imaginal discs (Men et al., 2016). In contrast *dPlin2* and human *PLIN2* and *3* are expressed ubiquitously (Itabe et al., 2017).

While the lipid storage function of LDs is well understood, less is known about the non-lipid storage functions of LDs, such as their involvement in the regulation of cellular stress and protein handling, folding, and turnover (Olzmann and Carvalho, 2019; Welte and Gould, 2017). This situation has improved in the last few years; for example, studies with *Drosophila* and vertebrate cellular models have begun to unravel the pathophysiological roles of LDs in regulating stress in cells of the nervous system. Oxidative stress exposure or excitotoxicity induces glial LD accumulation in developing or adult *Drosophila* and in mouse glial cells co-cultured with neurons (Bailey et al., 2015; Ioannou et al., 2019; Liu et al., 2015, 2017; Van Den Brink et al., 2018). In *Drosophila* larvae subjected to hypoxia, LD accumulation in glial cells is thought to play a neuroprotective role by enabling relocation of lipids sensitive to peroxidation, such as polyunsaturated FAs, from membrane phospholipids to TGs in the LD core (Bailey et al., 2015). In contrast with glial cells, LDs are rarely detected in neurons and little is known about their potential pathophysiological relevance of neuronal LDs to neurological diseases (Van Den Brink et al., 2018; Welte, 2015). Furthermore, LD biogenesis in glia, like in adipose tissue cells, depends on canonical enzymes such as Mdy (Bailey et al., 2015; Liu et al., 2015; Van Den Brink et al., 2018), while the mechanisms regulating their turnover in neurons are unknown.

PD is characterized by the neuronal accumulation of misfolded proteins, including α-synuclein (αSyn), in cytoplasmic aggregates known as Lewy bodies (Poewe et al., 2017; Shahmoradian et al., 2019). αSyn is a vertebrate-specific 14-kDa presynaptic protein and contains an N-terminal domain consisting of repeated sequences of 11 amino acids that fold into an amphipathic helix upon lipid binding (Bussell and Eliezer, 2003; Giménez-Andrés et al., 2018). Although the physiological function of αSyn is still unclear, several lines of evidence indicate that αSyn binding to phospholipid membranes is important for vesicle dynamics at the synapse (Auluck et al., 2010). And a recent study showed that the docking of synaptic vesicles to presynaptic membranes by αSyn depends on lipid composition (Man et al., 2021). Regarding PD, multiple lines of evidence indicate that lipid dysregulations are associated with

the disease. In particular, several genome wide association studies have identified genes regulating lipid metabolism as PD risk factors (Klemann et al., 2017). Also, mutations in glucocerebrosidase (GCase) gene is the highest risk factor of developing PD. The mutations of GCase gene are associated with a decrease in GCase activity leading to the accumulation of both glucosylceramide and αSyn (Muñoz et al., 2021). In a *Drosophila* model carrying a GCase mutation and expressing human αSyn, it was proposed that the binding of lipids to αSyn contributes to its pathogenic conversion (Suzuki et al., 2015). Furthermore, in yeast and mammalian cellular models of PD, the overexpression of αSyn leads to neutral lipids accumulation and LD formation (Cole et al., 2002; Fanning et al., 2019; Outeiro and Lindquist, 2003). It was initially proposed that αSyn could promote LD formation by inhibiting lipolysis at the surface of LDs (Cole et al., 2002). This hypothesis is supported by several studies showing that αSyn binds to LDs in mammalian cell cultures and synthetic LDs leading to the assumption that αSyn, similarly to perilipins, is as a *bonafide* LD protein (Cole et al., 2002; Čopič et al., 2018; Thiam et al., 2013). Alternatively, it was proposed that αSyn expression induces the accumulation of oleic acid generated by a stearoyl-CoA-desaturase enzyme, which fuels the synthesis of DGs and TGs to promote LD formation (Fanning et al., 2019). However, there is currently no animal model of PD, in which LD accumulation was observed preventing the investigation of a putative bidirectional interplay between αSyn and LDs *in vivo*.

In the present study, we used a *Drosophila* model in which the neuronal expression of human αSyn has proven to be useful to study the pathological mechanisms of PD (Auluck et al., 2002; Feany and Bender, 2000; Ordonez et al., 2018). We investigated the effects of PLIN and αSyn expression on LDs formation in photoreceptor neurons; the role of canonical mechanisms regulating LD metabolism; the subcellular co-localization of αSyn with LDs; the potential contribution of αSyn with several LD proteins to LD formation via the inhibition of lipolysis; and the potential effects of αSyn–LD binding on the susceptibility of αSyn to misfolding in the context of PD.

Results

Distinct anabolic and catabolic mechanisms regulate LD turnover in neurons and in glial cells

LDs are commonly observed and studied in glial cells but rarely in neurons in physiological or pathological conditions (Bailey et al., 2015; Liu et al., 2015; Van Den Brink et al., 2018). We hypothesized that the apparent lack of LD might be due to active lipolysis in neurons. We thus tested if the neuronal overexpression of PLIN proteins, which are regulating the access of lipases to LDs (Sztalryd and Brasaemle, 2017), could promote the neuronal accumulation of LDs. We focused on photoreceptor neurons of the *Drosophila* eye as a model. The compound eye of *Drosophila* is composed of 800 ommatidia, each containing six outer and two inner photoreceptor neurons surrounded by retina pigment/glial cells (Figure S1A-C) (Mollereau and Domingos, 2005). *dPlin1::GFP* (Beller et al., 2010) and *dPlin2::GFP* (Grönke et al., 2003) were expressed in outer photoreceptor neurons of the adult *Drosophila* using a rhodopsin 1 (*Rh1*) driver (Mollereau et al., 2000) and Figure S1D). The abundance of LDs was measured by labeling whole-mount retinas with the lipophilic fluorescent dye Bodipy. This analysis revealed that, while LDs were virtually undetectable in the retina of 20-day-old control flies, *dPlin1::GFP* or *dPlin2::GFP* overexpression led to accumulation of LDs (measured as the percentage of the retina area stained with Bodipy, Figure 1A and 1B). Next, we determined whether this effect of PLIN expression was specific to neurons or also observed in surrounding glial cells due to a non-autonomous effect. We thus immunostained the retina for the Na^+/K^+ ATPase α subunit, a marker of the photoreceptor plasma membrane (Yasuhara et al., 2000), which localization is depicted in cyan in the ommatidia diagram (Figure 1C). As shown in Figure 1D, *dPlin1::GFP* and *dPlin2::GFP* labeling was visible as rings, characteristic of proteins associated with the LD surface, located within the cytoplasm of photoreceptors but not in the adjacent glial cells. These results indicate that *Rh1*-driven PLIN overexpression, leads to accumulation of LDs in photoreceptor neurons only.

We then asked if LD biogenesis requires Mdy and dFatp, two canonical enzymes of the TG synthesis, in neurons as in glial cells. Photoreceptor neuron-specific knockdown of either *dFatp* or *Mdy* had no effect on LD accumulation in *dPlin1::GFP*-expressing flies (Figure 2A and 2B). To confirm these results, we performed loss of *dFatp* and *Mdy* function analyses in *dPlin*-expressing flies. *dPlin1*- or *dPlin2*-induced LDs in photoreceptors were not impacted neither by the loss of *dFatp* (*dFatp*$^{[k10307]}$) in FLP-mediated FRT-clones nor in *Mdy* (*Mdy*$^{[QX25]}$) mutant

(Figure 2C-2E, S2A and S2B). These results indicate that PLIN-induced LD accumulation in photoreceptor neurons occurs through a mechanism independent of *dFatp*- and *Mdy*-mediated *de novo* TG synthesis and is thus distinct from the mechanism of LD accumulation in glial cells.

Because PLINs are known to protect LDs from lipase-mediated lipolysis (Brasaemle, 2007), we examined whether the loss of lipolysis could be responsible for the accumulation of LDs. For that we first depleted main TG lipase Bmm, by RNAi interference, using the photoreceptor-specific *(Rh1-GAL4*) or the glial-specific (*54C-GAL4*) drivers. Photoreceptor-specific knockdown of *Bmm* did not increase LD abundance, suggesting that Bmm-mediated lipolysis does not influence LD homeostasis in photoreceptor neurons (Figure 2F). In contrast, knockdown of *Bmm* in glial cells resulted in LD accumulation (Figure 2F). These results were confirmed by observing that LD accumulate in glial but not in photoreceptor cells in *Bmm* mutant retina or in a pan-retinal *Bmm* knockdown (Figure 2G, S3A and S3B). The fact that LD degradation in *Drosophila* photoreceptor neurons does not involve Bmm, the main *Drosophila* TG lipase, is in contrast with what is observed in other tissues (Grönke et al., 2005). It suggests that an unknown lipase regulates the degradation of LDs in photoreceptors.

αSyn synergizes with PLIN protein to induce LD accumulation in neurons

Having established that PLIN levels regulate LD accumulation in neurons, we asked whether the expression of αSyn, which was proposed to interact with LDs as a *bonafide* LD protein (Cole et al., 2002; Čopič et al., 2018; Thiam et al., 2013), affected LD accumulation in photoreceptor neurons as well. For this, we employed transgenic *Drosophila* lines expressing wild-type human αSyn (Auluck et al., 2002; Chouhan et al., 2016; Cooper et al., 2006; Feany and Bender, 2000; Lessing and Bonini, 2009; Ordonez et al., 2018) alone or in combination with *dPlin1::GFP* or *dPlin2::GF*P. Notably, while photoreceptor neuron-specific expression of *αSyn* did not induce a significant LD accumulation compared with control (LacZ) flies, concomitant expression of *αSyn* and *dPlin2::GFP* resulted in a striking synergistic effect, more than tripling the abundance of LDs in photoreceptors compared with either *αSyn* or *dPlin2::GFP* expression alone (Figure 3A, 3B and 3C). This result was confirmed using independent fly lines carrying *UAS-dPlin2::GFP* and *UAS-αSyn* transgenes inserted at a different chromosomal localization (Figure S4A and S4B). Finally, we could also observed a synergistic accumulation of LDs induced with *αSyn* and *dPlin1::GFP* (Figure S5). Thus, while

Drosophila photoreceptor neurons contain few LDs under normal physiological conditions, the co-expression of *dPlin1* or *dPlin2* with *αSyn* increased LD content in a synergistic manner. These results suggest that *αSyn* functions in PLIN-like manner and could shield LDs, thus limiting the access of lipase and lipolysis.

αSyn and PLINs co-localize at the LD surface in *Drosophila* photoreceptor neurons and in human neuroblastoma cells

αSyn was found to bind LDs in several cellular models of PD transfected with *αSyn* protein (Cole et al., 2002; Fanning et al., 2019), but there is still no evidence that *αSyn* binds LDs in neurons in a model organism of PD. In addition, a putative binding of endogenous *αSyn* to LDs remains to be shown. We first performed Immunostaining of αSyn in flies with photoreceptor neuron-specific expression of *dPlin2::GFP* and αSyn, which revealed co-localization of the αSyn and dPlin2 at the LD surface (Figure 4A). In addition, we examined protein co-localization in the human neuroblastoma cell line SH-SY5Y transfected or not with *αSyn*. Transfected αSyn co-localized with PLIN3 (also known as TIP47), which is broadly expressed in human brain cells (Sjöstedt et al., 2020), around circular vesicles, as detected using high-resolution Airyscan microscopy (Figure 4B). Interestingly, αSyn distribution was not uniform and localized in subdomains at the LD surface. In non-transfected SH-SY5Y cells, the endogenous *αSyn* is expressed at low levels (Lee and Kamitani, 2011), we thus enhanced endogenous *αSyn* detection by performing proximity ligation assays (PLA), in which oligonucleotide-coupled secondary antibodies generate a fluorescent signal when the two target protein-bound primary antibodies are in close proximity (Wang et al., 2015). Confocal microscopy of non-transfected SH-SY5Y cells labeled with primary antibodies against αSyn and PLIN3 revealed PLA signals that localized around Bodipy-positive structures, indicating that endogenous αSyn and PLIN3 proteins co-localize at the surface of LDs (Figures 4C, S6A and S6B). A more robust PLA signal was observed in SH-SY5Y cells transfected with αSyn confirming the cellular localization of αSyn at the LDs (Figures 4D, S6C and S6D). Taken together, these experiments show that αSyn co-localizes at the LD surface with the LD-binding protein dPlin2 in *Drosophila* photoreceptor neurons and with PLIN3 in human neuroblastoma cells.

aSyn has a synergistic effect on LD accumulation with CG7900, a novel LD associated-protein in *Drosophila*

PLINs and αSyn overexpression promotes LD accumulation in a synergistic manner in *Drosophila* photoreceptor neurons. The fact that αSyn and PLINs co-localize at the surface of LDs raises the possibility that LDs should first be coated by PLIN before αSyn could bind at their surface. Alternatively, the LDs could serve as a physical platform, independently of PLIN, for αSyn to bind and to enhance LD accumulation. To test the latter, we asked if other LD proteins could promote LD accumulation synergistically with αSyn as well. We first characterized the cellular localization of CG7900, the *Drosophila* ortholog of FA amide hydrolase *FAAH2*, which contains a functional LD-binding domain (Kaczocha et al., 2010) and that we named *Drosophila* Faah2 (dFaah2). For that we used the larval fat body which contains large LDs (Beller et al., 2010). We generated a *Drosophila* transgenic UAS-CG7900-GFP line that we first expressed under the control of the larval fat body driver (*r4-GAL4*). We observed a clear localization of CG7900-GFP as a ring around LDs, which is characteristic of LD-binding proteins (Figure 5A) and indicates that CG7900 is a *bonafide* LD protein. We next asked if CG7900 overexpression is sufficient to induce the accumulation of LDs in photoreceptors. We observed that indeed the overexpression of CG7900-GFP using the Rh1 photoreceptor driver led to ring shapes in the photoreceptor cytoplasm, very similar to the expression of PLIN, suggesting an accumulation of LDs (Figure 5B). Interestingly the fact that the overexpression of several LD proteins (CG7900, dPlin1 or dPlin2) induce LDs suggest that LD accumulation is due to the shielding of LDs by LD proteins in photoreceptors. To test this hypothesis, we examined *Drosophila* expressing a fusion protein of GFP bound to the LD-binding domain (LD^{BD}-GFP) of the Nesprin family protein Klarsicht, that is required for the intracellular transport of LDs in *Drosophila* embryos (Welte et al., 1998; Yu et al., 2011). Notably, photoreceptor-specific expression of *LD^{BD}-GFP* induced an accumulation of LDs (Figure 5C, 5D and S7), similar to that observed with PLIN or CG7900 overexpression. Collectively, these results indicate that the shielding of LDs by LD protein promotes LD accumulation in neurons, presumably by keeping away an active lipase or by stabilizing their structure.

We next examined the consequence of co-expression of CG7900 or *LD^{BD}-GFP* and αSyn on LD accumulation. We found that αSyn expression enhanced synergistically the accumulation of LDs induced by CG7900 or *LD^{BD}-GFP* (Figure 5C, 5D). These last results further support the

hypothesis that distinct LD proteins by shielding the LDs from lipase, initiate LD accumulation, providing the appropriate surface for αSyn to bind and to enhance LD accumulation.

Finally, to further characterize the effect of CG7900 overexpression on LDs, we took advantage of a *UAS-αSyn^{A53T}* transgenic line, in which the insertion of αSyn^{A53T} occurs in the promoter region of *CG7900* (Figure S8A, chromosomal position 3R-48; see Materials and Methods). As shown in figure S8B, GAL4-mediated transcription of *UAS-αSyn^{A53T}* using the *GMR-GAL4* driver resulted in overexpression of *CG7900* (Figure S8B). This also resulted in the accumulation of LDs in photoreceptors, as visualized by Bodipy staining and transmission electronic microscopy (Figure S8C and S8D). Knockdown of *CG7900* in the *αSyn^{A53T}-CG7900* transgenic line abolished the accumulation of LDs (Figure S8E and S8F), indicating that in these conditions as well, CG7900 is required for LD accumulation in photoreceptors. Interestingly, lipidomic analyses of retinas revealed that only TGs were enriched, but no other lipid and sterol content, in flies with photoreceptor neuron-specific expression of *αSyn^{A53T}-CG7900* compared to wild type *αSyn* (*αSyn^{WT}*) or control flies (Figure S9). This suggests that LDs accumulating in photoreceptors contain TG and not sterol esters. Consistent with this, LD staining with Bodipy was abolished by overexpressing the TG lipase *Bmm* in *αSyn^{A53T}- CG7900* expressing flies (Figure S10A and S10B). These results demonstrate that TG is the major lipid in ectopic LD-induced by CG7900 and *αSyn^{A53T}*. Collectively these results support the fact that LD-binding proteins can act synergistically with αSyn to induce LD accumulation in photoreceptor neurons.

LDs promote αSyn resistance to proteinase K

In human neurons, αSyn aggregation is a multi-step process involving accumulation of misfolded αSyn, a process that renders αSyn resistant to mild proteolysis using proteinase K (Cremades et al., 2012; Suzuki et al., 2015). Therefore, we investigated whether αSyn–LD interactions might influence the physical state/structure of αSyn in *Drosophila* photoreceptor neurons. αSyn resistance to proteinase K was first evaluated by western blot analysis of protein extracts from flies overexpressing *αSyn^{WT}* or *dPlin2* and *αSyn^{WT}*. We observed that *αSyn* from 30-day-old transgenic flies was more resistant to proteinase K digestion with the concomitant expression of dPlin2 in which LDs accumulate (Figure 6A-6B), providing a direct link between LD abundance and aberrant αSyn folding and/or aggregation. To confirm this

link, we performed proteinase K-resistance assays on αSyn^{A53T}-CG7900 from 30-day-old flies depleted of LDs by co-expression of Bmm lipase in photoreceptor neurons. Indeed, depletion of LDs significantly reduced αSyn^{A53T} resistance to proteinase K digestion (Figure 6C and 6D), This indicates that LD abundance had a crucial influence on αSyn proteinase K-resistance. Taken together, these results support our conclusion that LD accumulation enhances the resistance of αSyn to proteinase K.

Discussion

In this study, we investigated the mechanisms that regulate LD homeostasis in neurons, the contribution of αSyn to LD homeostasis, and whether αSyn–LD binding influences the pathogenic potential of αSyn. We found that expression of the LD binding proteins, dPlin1 and dPlin2, CG7900 or of the LD-binding domain of Klarsicht increased LD accumulation in *Drosophila* photoreceptor neurons and that this phenotype was amplified by co-expressing the PD-associated protein αSyn. Transfected and endogenous αSyn co-localized with PLINs on the LD surface in human neuroblastoma cells, as demonstrated by confocal microscopy and PLA assays. PLIN-induced LD accumulation was not dependent on the canonical enzymes of TG synthesis (Mdy, dFatp) or ATGL/Bmm-dependant lipolysis inhibition, suggesting that LD binding proteins inhibit an unknown lipase in photoreceptor neurons. Finally, we observed that LD accumulation in photoreceptor neurons was associated with an increase resistance of αSyn to proteinase K, suggesting that LD accumulation might promote αSyn misfolding, an important step in the progression toward PD. Thus, we have uncovered a potential novel role for LDs in the pathogenicity of αSyn in PD.

Our understanding of the mechanisms of LD homeostasis in neurons under physiological or pathological conditions is far from complete. Neurons predominantly synthesize ATP through aerobic metabolism of glucose, rather than through FA β-oxidation, which likely explains the relative scarcity of LDs in neurons compared with glial cells (Schönfeld and Reiser, 2013). Here we used the *Drosophila* adult retina that is composed of photoreceptor neurons and glial cells to explore the mechanism regulating LD homeostasis in the nervous system. The canonical mechanisms regulating TG turnover and LD formation are dependent on evolutionary conserved regulators of lipogenesis and lipolysis in the fly adipose tissue, called fat body, or in other non-fat cells, such as glial cells (Heier and Kühnlein, 2018; Van Den Brink et al., 2018). Indeed, we and others showed that *de novo* TG-synthesis enzymes DGAT1/Mdy and dFatp, are required for LD biogenesis in the fat body and glial cells (Beller et al., 2010; Buszczak et al., 2002; Liu et al., 2015, 2017; Van Den Brink et al., 2018). This is in contrast with PLIN-induced neuronal accumulation of LDs (this study), which occurs through a non-canonical mechanism, independent of Mdy- and dFatp-mediated *de novo* TG synthesis. One possibility is that LD biogenesis depends on DGAT2 in neurons. However, the fact that DGAT2 is triplicated in the fly genome (Heier and Kühnlein, 2018) and that no triple mutant is available, precluded its functional analysis in the current study.

The evolutionarily conserved and canonical TG lipase Bmm, otholog of mammalian adipose triglyceride lipase (ATGL) regulates lipolysis in the fat body (Grönke et al., 2005). Here, we show that Bmm regulates lipolysis in glial cells but not in photoreceptor neurons. Interestingly, in both Bmm-mutant *Drosophila* (this study) and ATGL-mutant mice (Etschmaier et al., 2011), neurons do not accumulate LDs. This suggests the existence of an unknown and possibly a cell type specific lipase regulating the degradation of LDs in neurons. This is supported by the fact that the overexpression of PLINs proteins, which are known inhibitors of lipolysis, promotes LD accumulation in photoreceptor neurons. In further support of a neuron-specific lipase, it was proposed that DDHD2 which is part of the iPLA1/PAPLA1 family and which mutations are associated with the human disease, hereditary spastic paraplegia (HSP), could be the main lipase regulating TG metabolism in the brain (Inloes et al., 2014). Finally, we cannot exclude the possibility that the overexpression LD proteins, such as PLINs but also CG7900 or the Klarsicht lipid-binding domain by shielding LD limits the access of lipases but also stabilizes the structure of LDs. Indeed, stabilization of LDs could well be an ancestral function of PLINs, as reported for yeast and *Drosophila* adipose tissue (Beller et al., 2010; Čopič et al., 2018; Gao et al., 2017). Thus, inhibiting lipolysis and/or stabilizing LDs, allows the unmasking of LDs, which would be otherwise actively degraded in photoreceptor neurons. This opens avenues to further study LDs homeostasis but also their pathophysiological role in diseases of the nervous system.

Earlier studies have observed the accumulation of LDs in cellular models of PD. For example, SH-SY5Y cells exposed to 1-methyl-4-phenyl-1,2,3,6-tetrahydropyridine (MPTP), a dopaminergic neurotoxin prodrug that causes PD-like symptoms in animal and cellular models (Han et al., 2018). In addition, studies in yeast, rat dopaminergic neurons, and human induced pluripotent stem cells have proposed that αSyn expression induces lipid dysregulation and LD accumulation, but the underlying mechanisms remained unclear (Fanning et al., 2019; Outeiro and Lindquist, 2003; Sánchez Campos et al., 2018). Low levels of αSyn accumulation were thought to perturb lipid homeostasis by enhancing unsaturated FA synthesis and the subsequent accumulation of diacylglycerols (DGs) and TGs. In the present study, we showed that αSyn expression alone did not enhance the accumulation of LDs but instead required concomitant overexpression of a LD protein. Moreover, αSyn expression alone had no effect on DG, TG, or LD content in *Drosophila* photoreceptor neurons, which indicates that αSyn-induced LDs are not due to an increased TG biosynthesis in this cellular context. Instead, the

fact that endogenous αSyn and PLIN3 proteins co-localized at the LD surface in human neuroblastoma cells, suggests that LD-associated αSyn have a direct physiological function in promoting neutral lipid accumulation by inhibiting lipolysis. This hypothesis is supported by experiments in HeLa cells transfected with αSyn, loaded with fatty acids, in which the overexpression of αSyn protected LDs from lipolysis (Cole et al., 2002).

Our results show that LDs contribute to αSyn conversion to proteinase K resistant forms, which indicates that LDs may be involved in the progression of PD pathology. This is an apparent discrepancy with the results in Fanning et al. (2019), in which LDs protect from lipotoxicity cells expressing αSyn. In this study the authors used cellular models including yeast cells, and rat cortical neuron primary cultures exposed or not to oleic acid. In such cellular context, they propose that αSyn induces the accumulation of toxic diacylglycerol (DG), which is subsequently converted to TG and sequestered into LDs. LDs are thus protective by allowing the sequestration of toxic lipids. In our study, realized in the fly retina, αSyn expression did not induce TG accumulation. In *Drosophila* nervous system, toxic DG may not reach sufficient level to promote photoreceptor toxicity. Interestingly, this difference allowed us to study the binding of αSyn to LD and examine their contribution to pathological conversion of αSyn, which was not explored in Fanning *et al.*. Indeed, our results suggest an alternative but not mutually exclusive role for LDs in promoting αSyn misfolding and conversion to a proteinase K-resistant forms. The increased LD surface could provide a physical platform for αSyn deposition and conversion. In support of this hypothesis, it was previously proposed that αSyn aggregation is facilitated in the presence of synthetic phospholipid vesicles (Galvagnion et al., 2015). Although our results point to a direct role of LDs on αSyn resistance to proteinase K digestion, we cannot exclude an indirect mechanism by which autophagy or reactive oxygen species levels would contribute to this phenomenon.

We showed that the accumulation of LD proteins, such as PLINs, is a prerequisite for the increased LD accumulation induced by αSyn in neurons. This raises the possibility that some physiological or pathological conditions will favor the accumulation of LD proteins and the neuronal accumulation of LDs. Interestingly, it was proposed that age-dependent accumulation of fat and dPlin2 is dependent on the histone deacetylase (HDAC6) in *Drosophila* (Yan et al., 2017). Moreover, an accumulation of LD-containing cells (lipid-laden cells), associated with PLIN2 expression, was observed in meningeal, cortical and neurogenic brain

regions of the aging mice (Shimabukuro et al., 2016). As an alternative putative mechanism regulating LD level, it was shown that targeted degradation of PLIN2 and PLIN3 occurs by chaperone-mediated autophagy (CMA) (Kaushik and Cuervo, 2015). Thus, in aging tissue with decreased HDAC6 or reduced basal CMA, the accumulation of PLINs may initiate LD accumulation, hence favoring αSyn-induced LD production. In our hands, mutations in the autophagy gene, Atg8, did not lead to LD accumulation in *Drosophila* retina (data not shown), thus a more systematic analysis will be required to identify the proteolytic mechanisms regulating PLINs degradation and LD accumulation in the aged *Drosophila* nervous system.

Based on a combination of our results and these observations, we propose a model of LD homeostasis in healthy and diseased neurons (Figure 7). In healthy neurons, relatively few LDs are detected due to a combination of low basal rate of TG synthesis and active lipolysis. In pathological conditions such as PD, possibly in combination with an age-dependent ectopic fat accumulation and PLINs protein increase (Conte et al., 2019; Yan et al., 2017), αSyn and PLINs could cooperate to limit lipolysis and promote the accumulation of LDs in neurons. This could sets a vicious cycle in which αSyn enhances PLIN-dependent LD stabilization, which, in turn, would increases αSyn conversion to a proteinase K-resistant form, culminating in αSyn aggregation and formation of cytoplasmic inclusion bodies. Collectively, our results raise the possibility that αSyn binding to LDs could be an important step in the pathogenesis of PD.

Material and Methods

Fly Stocks

All flies used for this study were raised on regular yeast medium at 25°C on a 12h light/dark cycle. The fly stocks were obtained as follows. *UAS-αSyn* (third chromosome insertion BL8146, used throughout the paper unless it is specified), *UAS-αSyn^{A53T}-CG7900* (BL8148), *UAS-Mdy-RNAi* (BL65963), *UAS-Bmm-RNAi* (BL25926), *UAS-GFP-shRNA* (BL41555), *sGMR-GAL4*, *Rh1-GAL4* (BL8688), *TH-GAL4* (Alex Whitworth/Léo Pallanck), *UAS-CG7900* (EY10020, BL17633), *UAS-LacZ* (BL1777), *r4-GAL4* (BL33832) were from Bloomington *Drosophila* Stock Center. *UAS-dFatp-RNAi* (100124), *UAS-LacZ-RNAi* (51446) and *UAS-CG7900-RNAi* (101025) were from Vienna *Drosophila* Resource Center. *UAS-dPlin1::GFP* (Beller et al., 2010), *UAS-dPlin2::GFP* (Grönke et al., 2003) (second and third chromosome insertions), *UAS-Bmm* as well as *Bmm^{1}* (Grönke et al., 2005) and *Mdy^{QX25}* (Buszczak et al., 2002) mutant flies were provided by R.P. Kühnlein (University of Graz); *UAS-LD^{BD}-GFP* was provided by M. Welte (Yu et al., 2011); and *UAS-αSyn* (second chromosome insertion) was provided by M.B. Feany.

FRT mediated d*Fatp* photoreceptor clones were generated as previously described (Gambis et al., 2011) by crossing the following genotypes: *Rh1-GAL4, ey-FLP; FRT40A tdTomato^{NinaC}/ Cyo;* and *FRT40A dFatp^{k10307}/Cyo; UAS-dPlin1::GFP/TM6B*.

Generation of UAS-CG7900::GFP transgenic line

CG7900 cDNA was cloned (NotI/ BamHI) into a pJFRC2 vector in frame with the eGFP coding sequence (Pfeiffer et al., 2010). Best Gene, Inc (CA, USA) generated transgenic lines using PhiC31 integrase mediated transgenesis. The vector DNA was injected in embryos carrying attP40 docking sites.

Cell Culture

The human neuroblastoma cell line SH-SY5Y was obtained from T. Baron (ANSES, Lyon, France) and transfected with 1 µg of a pcDNA3.1 vector containing human αSyn cDNA (provided by T. Baron, Anses, Lyon, France) using Effecten transfection reagent (Qiagen). Positive clones were selected using geneticin and cultured in Dulbecco's modified Eagle's medium (DMEM/F-12, Gibco) supplemented with 4.5 g/L D-glucose, 10% fetal bovine serum, 100 U/mL penicillin, and 100 g/mL streptomycin at 37°C. Cells were passaged when they reached 70–80% confluence.

Bodipy Staining

Unless otherwise stated, experiments were performed using 20-day-old female flies. Flies were sedated on ice, decapitated, and the retinas were dissected in a drop of HL3 medium (Stewart et al., 1994). Whole-mount retinas were fixed in 4% paraformaldehyde (PFA), briefly washed in PBS supplemented with 0.1% Triton X-100 (PBS-T), and incubated overnight at 4°C in LD fluorescent dye Bodipy 493/503 (D3922, Molecular Probes) diluted in PBS-T supplemented with 1:400 phalloidin-rhodamine (R415, Molecular Probes) to label F-actin containing rhabdomeres. The retinas were rinsed once in PBS-T and then mounted on a bridged slide in Vectashield medium. Samples were examined on a Zeiss LSM800 at the LYMIC-PLATIM – Imaging and Microscopy Core Facility of SFR Biosciences (UMS3444), Lyon, France.

Bodipy Quantification

Retina images were acquired on a Zeiss LSM800 confocal microscope as 16-bit stacks and processed for quantification using ImageJ software (Schneider et al., 2012). Images were first filtered for noise using Gaussian Blur 3D (σ = 1) and projected along the Z-axis. LDs were identified using the Otsu thresholding algorithm. The area of Bodipy staining was measured and divided by the total retinal area as previously described (Van Den Brink et al., 2018).

Immunohistochemistry

Flies were sedated on ice, decapitated, and retinas were dissected in a drop of HL3 medium (Stewart et al., 1994) supplemented with D-glucose (120 mM). Whole-mount retinas were fixed in 4% PFA and permeabilized in PBS supplemented with 0.5% Triton X-100 and 5 mg/mL BSA. Mouse anti-Na+/K+ ATPase α-subunit (a5, DSHB), rabbit anti-GFP (A6455, Invitrogen), mouse anti-αSyn (sc-12767, Santa Cruz Biotechnology), or rabbit anti-dPlin2 (Grönke et al., 2003) a gift from R.P. Kühnlein) primary antibodies were diluted in blocking solution (PBS 1X, 0.5% Triton X-100, 5 mg/mL BSA and 4% Normal Goat Serum) and incubated with the retinas overnight at 4°C. The samples were then washed and incubated overnight at 4°C in blocking solution containing Alexa Fluor-conjugated anti-mouse Alexa488, anti-rabbit Alexa488, or anti-mouse Alexa647 secondary antibodies together with 1:400 phalloidin-rhodamine (R415, Molecular Probes) to label F-actin.

SH-SY5Y cells were fixed with 4% PFA for 15 min and permeabilized with PBS containing 5% BSA and 0.05% saponin for 15 min. Cells were then incubated with mouse anti-αSyn (1:2000,

sc-12767, Santa Cruz Biotechnology) and rabbit anti-PLIN3 (1:500, NB110, Novus Biologicals) primary antibodies at room temperature for 1 h. The cells were then washed and incubated with Bodipy 493/503 (D3922, Molecular Probes) and Alexa Fluor-conjugated anti-rabbit Alexa488/Alexa546 or anti-mouse Alexa647 secondary antibodies. Nuclei were counterstained with 1 µg/mL DAPI. Slides were mounted in Mowiol 4-88 (Sigma-Aldrich) and imaged with a Zeiss LSM800 confocal microscope.

Proximity Ligation Assay (PLA)

PLAs were performed using Duolink® PLA kits (Sigma) according to the manufacturer's instructions. Briefly, cells were fixed in 4% PFA and incubated with mouse anti-αSyn (1:2000, sc-12767, Santa Cruz Biotechnology) and rabbit anti-PLIN3 (1:500, NB110, Novus Biologicals) antibodies diluted in PBS containing 5% BSA and 0.05% saponin. The cells were then incubated with Duolink probes (anti-rabbit plus, DIO88002 and anti-mouse minus DIO82004).The PLA signal was revealed using the red Duolink In Situ Detection Reagent (DUO92008) and the cells were stained with Bodipy 493/503 (D3922, Molecular Probes). Nuclei were counterstained with DAPI in Mowiol mounting medium.

Mapping of *UAS-αSyn^{A53T}* Insertion Site

UAS-αSyn^{A53T} genomic localization was mapped using the Splinkerette protocol for mapping of transposable elements in *Drosophila* (Potter and Luo, 2010). Briefly, genomic DNA was isolated from one fly (stock BL8148) and digested using BstYI. DNA fragments containing the P-element flanking regions were then amplified using primers specific for pCaSpeR based P-element. The resulting DNA fragments were sequenced and mapped to the *Drosophila* genome using the BLAST platform.

Transmission Electron Microscopy (TEM) of *Drosophila* Eyes

TEM sample preparation was performed as previously described (Van Den Brink et al., 2018). Briefly, *Drosophila* eyes were fixed in 0.1 M cacodylate buffer supplemented with 2.5% glutaraldehyde and 2 mM $CaCl_2$ for 16 h at 4°C. After rinsing with 0.1 M cacodylate, the tissues were contrasted by incubation in 1% OsO_4 in 0.1 M cacodylate buffer for 2 h at room temperature. Tissues were then dehydrated in acetone and mounted in 100% epoxy resin

(Epon 812). After resin polymerization, samples were sliced into 60 nm sections, stained with lead citrate, and examined with a Philips CM120 TEM operating at 80 kV.

Lipid Extraction and Quantification by Shotgun Mass Spectrometry

Ten retinas per biological sample were homogenized twice for 5 min each with 1 mm zirconia beads in 300 µl isopropanol using a cooled Tissuelyzer II at 30 Hz. The homogenate was evaporated in a vacuum desiccator to complete dryness, and lipids were extracted as described (Knittelfelder et al., 2020; Sales et al., 2017). After evaporation, the samples were reconstituted in 300 µL 1:2 $CHCl_3$:MeOH. To quantify sterols, 200 µL aliquots of lipid extracts were evaporated and acetylated with 300 µL 2:1 $CHCl_3$:acetyl chloride for 1 h at room temperature (method modified from (Liebisch et al., 2006)). After evaporation, sterol samples were reconstituted in 200 µL 4:2:1 isopropanol:MeOH:$CHCl_3$ with 7.5 mM ammonium formate (spray solution). For sterol and lipidome measurements, samples were diluted 1:1 with spray solution. Mass spectrometric analysis was performed as described (Knittelfelder et al., 2020).

RNA Extraction and qRT-PCR

Total RNA was extracted from three sets of 10 *Drosophila* heads using TRI-Reagent (T9424, Sigma) and RNA was reverse transcribed using an iScript cDNA Synthesis Kit (Bio-Rad) according to the manufacturers' instructions. Quantitative PCR reactions were carried out using FastStart Universal SYBER Green Master mix (Roche Applied Science) on a StepOnePlus system (Applied Biosystems). Primer efficiency (E) was assessed using serial dilutions of cDNA preparations. Standard curves were used to determine the relationship between PCR cycle number (Ct) and mRNA abundance. Relative mRNA quantity (Qr) was calculated as: Qr = $E^{\wedge}Ct_{Rp49}$-Ct_{target}. Qr values were then normalized to control genotype. Experiments were performed using the following primers: *CG7900*: 5'-CTGCTCACTCTCAGCGTTCAG-3' and 5'-ATATGTGCGAACCAACTCCAC-3'; *Rp49*: 5'-ATCGTGAAGAAGCGCACCAAG-3' and 5'-ACCAGGAACTTCTTGAATCCG-3'.

Proteinase K-Resistance Assay

Fly heads were homogenized in lysis buffer (50 mM Tris-HCl pH 7.5, 5 mM EDTA, 0.1% NP40, 1 mM DTT, and 1% Protease Inhibitor Cocktail), incubated for 1 h at 25°C, and centrifuged at

13,000 rpm for 1 min. Supernatants were collected and incubated for 30 min at 25°C with proteinase K (0, 0.5, 1, 1.5, or 2 µg/mL). Denaturing buffer TD4215 4X was added to each sample, and proteins were separated in 4%–15% gradient acrylamide gels (Bio-Rad) and transferred to PVDF membranes (Millipore). PVDF membranes were fixed in 4% PFA and 0.01% glutaraldehyde in PBS for 30 min and then blocked in 3% BSA/0.1% Tween/PBS for 1h. Membranes were incubated with rabbit anti-α-Syn (MJFR1, ab138501, Abcam; 1:1000) or mouse anti-β-tubulin (T 6199, Sigma, 1:1000) primary antibodies overnight at 4°C, washed, and incubated with horseradish peroxidase-conjugated anti-mouse IgG or anti-rabbit IgG (both from Pierce, 1:1000). After washing, membranes were incubated with SuperSignal West Dura Chemiluminescence Substrate (Thermo Scientific), and images were acquired using a ChemiDoc MP system (Bio-Rad).

Statistical Analysis

Data are presented as the means ± standard deviation (SD) of three experiments unless noted. Statistical analyses were performed using R software. Differences between groups were analyzed by t-test or ANOVA and Tukey's HSD paired sample comparison test depending on the number of groups, as specified in the figure legends.

Acknowledgements

We thank the ARTHRO-TOOLS and LYMIC-PLATIM microscopy platforms of SFR Biosciences (UMS3444/CNRS, US8/INSERM, ENS de Lyon, UCBL) and the Centre Technologique des Microstructures CTµ at Lyon 1 University. We thank our colleagues and the stock fly centers for kindly sending fly stocks. This work was supported by grants from ENS Fond Recherche and the Association France Parkinson to BM. VG was supported by the Laboratory of Modelling and Biology of the Cell, Servier Research Institute, a PhD fellowship from Fondation pour la Recherche Medicale, and salary support from ENS Fond Recherche. Work in the Shevchenko laboratory was supported by Deutsche Forschungsgemeinschaft (grant FOR 2682).

Author Contribution

VG, ND, DVB, and BM designed the experiments and interpreted the results. BM obtained funding to support this research. VG performed most of the experiments with the contribution of others as followed: FJ performed the mammalian cell experiments with the help of VG, GC,

performed the electronic microscopy. VG performed the proteinase K resistance assay with the help of JNA in TB's laboratory. O.K. performed the mass spectrometry lipidomic analysis in AS's laboratory. VG performed all statistical analysis. VG prepared the figures and drawings. VG and BM wrote the first draft of the manuscript. VG, ND and BM revised the manuscript for critical content.

Conflicts of Interest

The authors declare that they have no competing interests.

Figure Legends

Figure 1. dPlin1 and dPlin2 promote LD accumulation in *Drosophila* photoreceptor neurons.

(A) LD staining of whole-mount retinas from flies expressing *GFP* (control), *dPlin1::GFP*, or *dPlin2::GFP* in photoreceptor neurons (*Rh1-GAL4*). LDs are in green (Bodipy) and photoreceptor rhabdomeres are in magenta (phalloidin-rhodamine). Scale bar, 10 µm.

(B) Quantification of LD area expressed as % of total retinal area. Data are from the images shown in (A). Mean ± SD. ***p<0.001 by ANOVA with Tukey's HSD test.

(C) Diagram of a longitudinal section of one ommatidium. Each ommatidium is composed of 8 photoreceptor neurons delimitated by a Na^+/K^+ ATPase positive plasma membrane (cyan), each containing one rhabdomere (magenta), and surrounded by 9 glial cells (also known as retinal pigment cells; light and dark gray).

(D) Immunostaining of whole-mount retinas from flies expressing *dPlin1::GFP* or *dPlin2::GFP* in photoreceptor neurons (*Rh1-GAL4*). Photoreceptor plasma membranes are in cyan (anti-Na^+/K^+ ATPase) and rhabdomeres are in magenta (phalloidin-rhodamine). dPlin1 and dPlin2 are visible as ring shapes in the photoreceptor cytoplasm (yellow arrowheads). Scale bar, 10 µm.

Figure 2. dPlin1-induced LDs in photoreceptor neurons do not require canonical enzymes involved in TG synthesis (*dFatp*, *Mdy*) or degradation (*Bmm*).

(A) LD staining of whole-mount retina from flies with photoreceptor neuron-specific (*Rh1-GAL4*) expression of *dPlin1::GFP* and *LacZ-RNAi* (control), *dFatp-RNAi,* or *Mdy-RNAi*. LDs are in green (Bodipy) and photoreceptor rhabdomeres are in magenta (phalloidin-rhodamine). Scale bar, 10 µm.

(B) Quantification of LD area from the images shown in (A). Mean ± SD. ns, not significant by ANOVA.

(C) Bodipy staining of whole-mount retinas from flipase mediated FRT *dFatp[k10307]* mutant clone in conjunction with expression of *dPlin1::GFP* in photoreceptor (*Rh1-GAL4*). LDs are in green (Bodipy), wild type photoreceptors are in grey (*FRT40A-Tomato[ninaC]*) and rhabdomeres are in magenta (phalloidin-rhodamine). LDs are visible in photoreceptors lacking *dFatp* (mutant clone surrounded by dashed line). Scale bar, 10 µm.

(D, E) whole-mount retinas from *mdy*$^{[QX25]}$ heterozygous and homozygous flies expressing *dPlin1::GFP* in photoreceptor (*Rh1-GAL4*). **(D)** LDs are in green (Bodipy), and rhabdomeres are in magenta (phalloidin-rhodamine). **(E)** Photoreceptor plasma membranes are in cyan (anti-Na^+/K^+ ATPase) and rhabdomeres are in magenta (phalloidin-rhodamine).

(F) LD staining of whole-mount retinas from *flies* expressing *Bmm lipase RNAi* in photoreceptor (Rh1-GAL4) or retina glia (54C-GAL4). LDs are in green (Bodipy), and rhabdomeres are in magenta (phalloidin-rhodamine).

(G) Immunostaining of whole-mount retinas from homozygous *Bmm[1]* mutant flies. Photoreceptor plasma membranes are in cyan (anti-Na^+/K^+ ATPase) and rhabdomeres are in magenta (phalloidin-rhodamine).

Figure 3. αSyn enhances dPlin2-induced LD accumulation in *Drosophila* photoreceptor neurons.

(A) LD staining of whole-mount retinas from flies expressing LacZ (control) or human αSyn alone or in conjunction with *dPlin2::GFP* in photoreceptor neurons (*Rh1-GAL4*). LDs are in green (Bodipy) and photoreceptor rhabdomeres are in magenta (phalloidin-rhodamine). Scale bar, 10 µm.

(B) Quantification of LD area expressed as % of total retinal area. Data are from the images shown in (A). Mean ± SD. ** $p<0.01$, ***$p<0.001$ by ANOVA with Tukey's HSD test.

(C) Immunostaining of whole-mount retinas from flies expressing *dPlin2::GFP* in photoreceptor neurons (*Rh1-GAL4*). Photoreceptor plasma membranes are in cyan (anti-Na^+/K^+ ATPase immunostaining) and rhabdomeres are in magenta (phalloidin-rhodamine labeling of F-actin). dPlin2 staining is visible as ring shapes in the photoreceptor cytoplasm (yellow arrowheads). Scale bar, 10 µm.

Figure 4. αSyn co-localizes with PLINs at the surface of LDs in *Drosophila* photoreceptor neurons and in human neuroblastoma cells.

(A) Immunostaining of whole-mount retinas from flies expressing αSyn and *dPlin2::GFP* in photoreceptor neurons (*Rh1-GAL4*). αSyn is in magenta (anti-αSyn) and photoreceptor rhabdomeres are in red (phalloidin-rhodamine). White arrowheads indicate co-localization of αSyn and dPlin2 at LDs. Scale bar, 5µm.

(B) High-resolution Airyscan micrograph of SH-SY5Y neuroblastoma cells transfected with αSyn. αSyn and PLIN3 immunostainings are shown in magenta and green, respectively. Nuclei are counterstained with DAPI (cyan). Arrowheads indicate co-localization of αSyn and PLIN3 staining on LDs. Scale bar, 5 µm.

(C) Proximity ligation assay between PLIN3 and endogenous αSyn in SH-SY5Y. The PLA signal generated by close proximity of the two protein-bound primary antibodies is shown in magenta, LDs are in green (Bodipy), and nuclei are counterstained with DAPI (cyan). Scale bars, 5 µm.

(D) Proximity ligation assay between αSyn and PLIN3 in SH-SY5Y cells transfected with human αSyn. The PLA signal generated by close proximity of the two protein-bound primary antibodies is shown in magenta, LDs are in green (Bodipy), and nuclei are counterstained with DAPI (cyan). Scale bars, 5 µm.

Figure 5. *CG7900* binds LDs in *Drosophila* tissues and promotes LD accumulation in photoreceptors

(A) Immunostaining of whole mount *Drosophila* larval fat body expressing CG7900::GFP (*r4-GAL4*). CG7900::GFP is in green and LDs stained by monodansylpenthane are in cyan. Scale bar, 20µm.

(B) Immunostaining of whole-mount retinas from flies expressing *CG7900::GFP* in photoreceptor neurons (*Rh1-GAL4*). Photoreceptor plasma membranes are in cyan (anti-Na^+/K^+ ATPase) and rhabdomeres are in magenta (phalloidin-rhodamine). Arrowheads indicate ring shaped GFP positive staining in photoreceptors. Scale bar, 10 µm.

(C) LD staining of whole-mount retina from flies with photoreceptor neuron-specific expression (*Rh1-GAL4*) of *LacZ* (control), *CG7900,* Klarsicht LD-binding domain (LD^{BD}-GFP), alone or in conjunction with αSyn. LDs are shown in green (Bodipy) and photoreceptor rhabdomeres in magenta (phalloidin-rhodamine). Scale bar, 10 µm.

(D) Quantification of LD area from the images shown in (E). Mean ± SD. * $p<0.05$, *** $p<0.001$ by ANOVA with Tukey's HSD test.

Figure 6. LDs promote αSyn resistance to proteinase K in *Drosophila* photoreceptors

(A) αSyn proteinase K-resistance assay. Lysates of the heads of 30-day-old flies with photoreceptor neuron-specific expression of *αSyn^{WT}* and either *LacZ* (control) or *dPlin2::GFP* were digested with the indicated concentrations of proteinase K and then immunoblotted for αSyn or β-tubulin (loading control).

(B) Quantification of proteinase K-resistant αSyn, as analyzed in (A). Resistance is expressed as the ratio of αSyn detected after treatment with 1 µg/mL of proteinase K relative to the untreated sample. Mean ± SD. * $p<0.05$ by student test.

(C) αSyn proteinase K-resistance assay. Lysates of the heads of 30-day-old flies with photoreceptor neuron-specific expression (*Rh1-GAL4*) of *αSyn^{A53T}-CG7900* and either *LacZ* (control) or *Bmm* lipase were digested with the indicated concentrations of proteinase K and then immunoblotted for αSyn or β-tubulin (loading control).

(D) Quantification of proteinase K-resistant αSyn, as analyzed in (B). Resistance is expressed as the ratio of αSyn detected after treatment with 2 µg/mL of proteinase K relative to the untreated sample.

Figure 7. Model of the reciprocal interactions between αSyn and LDs in PD.

Under normal physiological conditions, neurons contain relatively few LDs. We propose the following scenario under pathological conditions associated with elevated levels of αSyn and dPlin2: **(1)** the increase dPlin2 limits the action of neuronal lipases and promotes LDs accumulation; **(2)** αSyn binds to the expanding dPlin2-positive LDs, which further increases LD accumulation; **(3)** αSyn is converted to a proteinase K-resistant form(s) on the surface of LDs; and **(4)** the aberrant form of αSyn may aggregate at the surface of or in close proximity to LDs, leading to formation of cytoplasmic inclusion bodies (Dettmer et al., 2017).

Bibliography

Auluck, P.K., Chan, H.Y.E., Trojanowski, J.Q., Lee, V.M.-Y., and Bonini, N.M. (2002). Chaperone Suppression of a-Synuclein Toxicity in a Drosophila Model for Parkinson's Disease. Science *295*, 862–865.

Auluck, P.K., Caraveo, G., and Lindquist, S. (2010). α-Synuclein: membrane interactions and toxicity in Parkinson's disease. Annu. Rev. Cell Dev. Biol. *26*, 211–233.

Bailey, A.P., Koster, G., Guillermier, C., Hirst, E.M.A., MacRae, J.I., Lechene, C.P., Postle, A.D., and Gould, A.P. (2015). Antioxidant Role for Lipid Droplets in a Stem Cell Niche of Drosophila. Cell *163*, 340–353.

Beller, M., Riedel, D., Jansch, L., Dieterich, G., Wehland, J., Jackle, H., and Kuhnlein, R.P. (2006). Characterization of the Drosophila Lipid Droplet Subproteome. Mol. Cell. Proteomics.

Beller, M., Bulankina, A.V., Hsiao, H.-H., Urlaub, H., Jäckle, H., and Kühnlein, R.P. (2010). PERILIPIN-Dependent Control of Lipid Droplet Structure and Fat Storage in Drosophila. Cell Metab. *12*, 521–532.

Bi, J., Xiang, Y., Chen, H., Liu, Z., Grönke, S., Kühnlein, R.P., and Huang, X. (2012). Opposite and redundant roles of the two Drosophila perilipins in lipid mobilization. J. Cell Sci. *125*, 3568–3577.

Brasaemle, D.L. (2007). Thematic review series: adipocyte biology. The perilipin family of structural lipid droplet proteins: stabilization of lipid droplets and control of lipolysis. J. Lipid Res. *48*, 2547–2559.

Bussell, R., and Eliezer, D. (2003). A Structural and Functional Role for 11-mer Repeats in α-Synuclein and Other Exchangeable Lipid Binding Proteins. J. Mol. Biol. *329*, 763–778.

Buszczak, M., Lu, X., Segraves, W.A., Chang, T.Y., and Cooley, L. (2002). Mutations in the midway gene disrupt a Drosophila acyl coenzyme A: diacylglycerol acyltransferase. Genetics *160*, 1511–1518.

Chouhan, A.K., Guo, C., Hsieh, Y.-C., Ye, H., Senturk, M., Zuo, Z., Li, Y., Chatterjee, S., Botas, J., Jackson, G.R., et al. (2016). Uncoupling neuronal death and dysfunction in Drosophila models of neurodegenerative disease. Acta Neuropathol. Commun. *4*.

Cole, N.B., Murphy, D.D., Grider, T., Rueter, S., Brasaemle, D., and Nussbaum, R.L. (2002). Lipid droplet binding and oligomerization properties of the Parkinson's disease protein alpha-synuclein. J. Biol. Chem. *277*, 6344–6352.

Conte, M., Martucci, M., Sandri, M., Franceschi, C., and Salvioli, S. (2019). The Dual Role of the Pervasive "Fattish" Tissue Remodeling With Age. Front. Endocrinol. *10*, 114.

Cooper, A.A., Gitler, A.D., Cashikar, A., Haynes, C.M., Hill, K.J., Bhullar, B., Liu, K., Xu, K., Strathearn, K.E., Liu, F., et al. (2006). α-Synuclein Blocks ER-Golgi Traffic and Rab1 Rescues Neuron Loss in Parkinson's Models. Science *313*, 324–328.

Čopič, A., Antoine-Bally, S., Giménez-Andrés, M., La Torre Garay, C., Antonny, B., Manni, M.M., Pagnotta, S., Guihot, J., and Jackson, C.L. (2018). A giant amphipathic helix from a perilipin that is adapted for coating lipid droplets. Nat. Commun. *9*.

Cremades, N., Cohen, S.I.A., Deas, E., Abramov, A.Y., Chen, A.Y., Orte, A., Sandal, M., Clarke, R.W., Dunne, P., Aprile, F.A., et al. (2012). Direct Observation of the Interconversion of Normal and Toxic Forms of α-Synuclein. Cell *149*, 1048–1059.

Dettmer, U., Ramalingam, N., von Saucken, V.E., Kim, T.-E., Newman, A.J., Terry-Kantor, E., Nuber, S., Ericsson, M., Fanning, S., Bartels, T., et al. (2017). Loss of native α-synuclein multimerization by strategically mutating its amphipathic helix causes abnormal vesicle interactions in neuronal cells. Hum. Mol. Genet. *26*, 3466–3481.

Dourlen, P., Sujkowski, A., Wessells, R., and Mollereau, B. (2015). Fatty acid transport proteins in disease: New insights from invertebrate models. Prog. Lipid Res. *60*, 30–40.

Etschmaier, K., Becker, T., Eichmann, T.O., Schweinzer, C., Scholler, M., Tam-Amersdorfer,

C., Poeckl, M., Schuligoi, R., Kober, A., Chirackal Manavalan, A.P., et al. (2011). Adipose triglyceride lipase affects triacylglycerol metabolism at brain barriers. J. Neurochem. *119*, 1016–1028.
Fanning, S., Haque, A., Imberdis, T., Baru, V., Barrasa, M.I., Nuber, S., Termine, D., Ramalingam, N., Ho, G.P.H., Noble, T., et al. (2019). Lipidomic Analysis of α-Synuclein Neurotoxicity Identifies Stearoyl CoA Desaturase as a Target for Parkinson Treatment. Mol. Cell *73*, 1001-1014.e8.
Fanning, S., Selkoe, D., and Dettmer, U. (2020). Parkinson's disease: proteinopathy or lipidopathy? NPJ Park. Dis. *6*, 3.
Farmer, B.C., Walsh, A.E., Kluemper, J.C., and Johnson, L.A. (2020). Lipid Droplets in Neurodegenerative Disorders. Front. Neurosci. *14*, 742.
Feany, M.B., and Bender, W.W. (2000). A Drosophila model of Parkinson's disease. Nature *404*, 394–398.
Galvagnion, C., Buell, A.K., Meisl, G., Michaels, T.C.T., Vendruscolo, M., Knowles, T.P.J., and Dobson, C.M. (2015). Lipid vesicles trigger α-synuclein aggregation by stimulating primary nucleation. Nat. Chem. Biol. *11*, 229–234.
Gambis, A., Dourlen, P., Steller, H., and Mollereau, B. (2011). Two-color in vivo imaging of photoreceptor apoptosis and development in Drosophila. Dev. Biol. *351*, 128–134.
Gao, Q., Binns, D.D., Kinch, L.N., Grishin, N.V., Ortiz, N., Chen, X., and Goodman, J.M. (2017). Pet10p is a yeast perilipin that stabilizes lipid droplets and promotes their assembly. J. Cell Biol. *216*, 3199–3217.
Giménez-Andrés, M., Čopič, A., and Antonny, B. (2018). The Many Faces of Amphipathic Helices. Biomolecules *8*.
Grönke, S., Beller, M., Fellert, S., Ramakrishnan, H., Jäckle, H., and Kühnlein, R.P. (2003). Control of fat storage by a Drosophila PAT domain protein. Curr. Biol. CB *13*, 603–606.
Grönke, S., Mildner, A., Fellert, S., Tennagels, N., Petry, S., Müller, G., Jäckle, H., and Kühnlein, R.P. (2005). Brummer lipase is an evolutionary conserved fat storage regulator in Drosophila. Cell Metab. *1*, 323–330.
Han, X., Zhu, J., Zhang, X., Song, Q., Ding, J., Lu, M., Sun, S., and Hu, G. (2018). Plin4-Dependent Lipid Droplets Hamper Neuronal Mitophagy in the MPTP/p-Induced Mouse Model of Parkinson's Disease. Front. Neurosci. *12*, 397.
Heier, C., and Kühnlein, R.P. (2018). Triacylglycerol Metabolism in Drosophila melanogaster. Genetics *210*, 1163–1184.
Inloes, J.M., Hsu, K.-L., Dix, M.M., Viader, A., Masuda, K., Takei, T., Wood, M.R., and Cravatt, B.F. (2014). The hereditary spastic paraplegia-related enzyme DDHD2 is a principal brain triglyceride lipase. Proc. Natl. Acad. Sci. U. S. A. *111*, 14924–14929.
Ioannou, M.S., Jackson, J., Sheu, S.-H., Chang, C.-L., Weigel, A.V., Liu, H., Pasolli, H.A., Xu, C.S., Pang, S., Matthies, D., et al. (2019). Neuron-Astrocyte Metabolic Coupling Protects against Activity-Induced Fatty Acid Toxicity. Cell *177*, 1522-1535.e14.
Itabe, H., Yamaguchi, T., Nimura, S., and Sasabe, N. (2017). Perilipins: a diversity of intracellular lipid droplet proteins. Lipids Health Dis. *16*, 83.
Jackson, C.L. (2019). Lipid droplet biogenesis. Curr. Opin. Cell Biol. *59*, 88–96.
Kaczocha, M., Glaser, S.T., Chae, J., Brown, D.A., and Deutsch, D.G. (2010). Lipid droplets are novel sites of N-acylethanolamine inactivation by fatty acid amide hydrolase-2. J. Biol. Chem. *285*, 2796–2806.
Kaushik, S., and Cuervo, A.M. (2015). Degradation of lipid droplet-associated proteins by chaperone-mediated autophagy facilitates lipolysis. Nat. Cell Biol. *17*, 759–770.
Kimmel, A.R., and Sztalryd, C. (2016). The Perilipins: Major Cytosolic Lipid Droplet-Associated Proteins and Their Roles in Cellular Lipid Storage, Mobilization, and Systemic Homeostasis. Annu. Rev. Nutr. *36*, 471–509.

Klemann, C.J.H.M., Martens, G.J.M., Sharma, M., Martens, M.B., Isacson, O., Gasser, T., Visser, J.E., and Poelmans, G. (2017). Integrated molecular landscape of Parkinson's disease. Npj Park. Dis. *3*, 14.
Knittelfelder, O., Prince, E., Sales, S., Fritzsche, E., Wöhner, T., Brankatschk, M., and Shevchenko, A. (2020). Sterols as dietary markers for Drosophila melanogaster. Biochim. Biophys. Acta Mol. Cell Biol. Lipids *1865*, 158683.
Krahmer, N., Farese, R.V., and Walther, T.C. (2013). Balancing the fat: lipid droplets and human disease. EMBO Mol. Med. *5*, 973–983.
Lee, B.R., and Kamitani, T. (2011). Improved Immunodetection of Endogenous α-Synuclein. PLOS ONE *6*, e23939.
Lessing, D., and Bonini, N.M. (2009). Maintaining the brain: insight into human neurodegeneration from Drosophila melanogaster mutants. Nat. Rev. Genet. *10*, 359–370.
Liebisch, G., Binder, M., Schifferer, R., Langmann, T., Schulz, B., and Schmitz, G. (2006). High throughput quantification of cholesterol and cholesteryl ester by electrospray ionization tandem mass spectrometry (ESI-MS/MS). Biochim. Biophys. Acta *1761*, 121–128.
Liu, L., Zhang, K., Sandoval, H., Yamamoto, S., Jaiswal, M., Sanz, E., Li, Z., Hui, J., Graham, B.H., Quintana, A., et al. (2015). Glial Lipid Droplets and ROS Induced by Mitochondrial Defects Promote Neurodegeneration. Cell *160*, 177–190.
Liu, L., MacKenzie, K.R., Putluri, N., Maletić-Savatić, M., and Bellen, H.J. (2017). The Glia-Neuron Lactate Shuttle and Elevated ROS Promote Lipid Synthesis in Neurons and Lipid Droplet Accumulation in Glia via APOE/D. Cell Metab. *26*, 719-737.e6.
Man, W.K., Tahirbegi, B., Vrettas, M.D., Preet, S., Ying, L., Vendruscolo, M., De Simone, A., and Fusco, G. (2021). The docking of synaptic vesicles on the presynaptic membrane induced by α-synuclein is modulated by lipid composition. Nat. Commun. *12*, 927.
Men, T.T., Binh, T.D., Yamaguchi, M., Huy, N.T., and Kamei, K. (2016). Function of Lipid Storage Droplet 1 (Lsd1) in Wing Development of Drosophila melanogaster. Int. J. Mol. Sci. *17*.
Mollereau, B., and Domingos, P.M. (2005). Photoreceptor differentiation in Drosophila: from immature neurons to functional photoreceptors. Dev. Dyn. Off. Publ. Am. Assoc. Anat. *232*, 585–592.
Mollereau, B., Wernet, M.F., Beaufils, P., Killian, D., Pichaud, F., Kühnlein, R., and Desplan, C. (2000). A green fluorescent protein enhancer trap screen in Drosophila photoreceptor cells. Mech. Dev. *93*, 151–160.
Muñoz, S.S., Petersen, D., Marlet, F.R., Kücükköse, E., and Galvagnion, C. (2021). The interplay between Glucocerebrosidase, α-synuclein and lipids in human models of Parkinson's disease. Biophys. Chem. *273*, 106534.
Olzmann, J.A., and Carvalho, P. (2019). Dynamics and functions of lipid droplets. Nat. Rev. Mol. Cell Biol. *20*, 137–155.
Ordonez, D.G., Lee, M.K., and Feany, M.B. (2018). α-synuclein Induces Mitochondrial Dysfunction through Spectrin and the Actin Cytoskeleton. Neuron *97*, 108-124.e6.
Outeiro, T.F., and Lindquist, S. (2003). Yeast cells provide insight into alpha-synuclein biology and pathobiology. Science *302*, 1772–1775.
Pennetta, G., and Welte, M.A. (2018). Emerging Links between Lipid Droplets and Motor Neuron Diseases. Dev. Cell *45*, 427–432.
Pfeiffer, B.D., Ngo, T.-T.B., Hibbard, K.L., Murphy, C., Jenett, A., Truman, J.W., and Rubin, G.M. (2010). Refinement of tools for targeted gene expression in Drosophila. Genetics *186*, 735–755.
Poewe, W., Seppi, K., Tanner, C.M., Halliday, G.M., Brundin, P., Volkmann, J., Schrag, A.-E., and Lang, A.E. (2017). Parkinson disease. Nat. Rev. Dis. Primer *3*, 17013.
Potter, C.J., and Luo, L. (2010). Splinkerette PCR for Mapping Transposable Elements in

Drosophila. PLoS ONE *5*, e10168.
Sales, S., Knittelfelder, O., and Shevchenko, A. (2017). Lipidomics of Human Blood Plasma by High-Resolution Shotgun Mass Spectrometry. In Methods in Molecular Biology, pp. 203–212.
Salo, V.T., Li, S., Vihinen, H., Hölttä-Vuori, M., Szkalisity, A., Horvath, P., Belevich, I., Peränen, J., Thiele, C., Somerharju, P., et al. (2019). Seipin Facilitates Triglyceride Flow to Lipid Droplet and Counteracts Droplet Ripening via Endoplasmic Reticulum Contact. Dev. Cell *50*, 478-493.e9.
Sánchez Campos, S., Alza, N.P., and Salvador, G.A. (2018). Lipid metabolism alterations in the neuronal response to A53T α-synuclein and Fe-induced injury. Arch. Biochem. Biophys. *655*, 43–54.
Schneider, C.A., Rasband, W.S., and Eliceiri, K.W. (2012). NIH Image to ImageJ: 25 years of Image Analysis. Nat. Methods *9*, 671–675.
Schönfeld, P., and Reiser, G. (2013). Why does brain metabolism not favor burning of fatty acids to provide energy? Reflections on disadvantages of the use of free fatty acids as fuel for brain. J. Cereb. Blood Flow Metab. Off. J. Int. Soc. Cereb. Blood Flow Metab. *33*, 1493–1499.
Shahmoradian, S.H., Lewis, A.J., Genoud, C., Hench, J., Moors, T.E., Navarro, P.P., Castaño-Díez, D., Schweighauser, G., Graff-Meyer, A., Goldie, K.N., et al. (2019). Lewy pathology in Parkinson's disease consists of crowded organelles and lipid membranes. Nat. Neurosci. *22*, 1099–1109.
Shimabukuro, M.K., Langhi, L.G.P., Cordeiro, I., Brito, J.M., Batista, C.M. de C., Mattson, M.P., and Mello Coelho, V. de (2016). Lipid-laden cells differentially distributed in the aging brain are functionally active and correspond to distinct phenotypes. Sci. Rep. *6*, 23795.
Sjöstedt, E., Zhong, W., Fagerberg, L., Karlsson, M., Mitsios, N., Adori, C., Oksvold, P., Edfors, F., Limiszewska, A., Hikmet, F., et al. (2020). An atlas of the protein-coding genes in the human, pig, and mouse brain. Science *367*.
Stewart, B.A., Atwood, H.L., Renger, J.J., Wang, J., and Wu, C.F. (1994). Improved stability of Drosophila larval neuromuscular preparations in haemolymph-like physiological solutions. J. Comp. Physiol. [A] *175*, 179–191.
Suzuki, M., Fujikake, N., Takeuchi, T., Kohyama-Koganeya, A., Nakajima, K., Hirabayashi, Y., Wada, K., and Nagai, Y. (2015). Glucocerebrosidase deficiency accelerates the accumulation of proteinase K-resistant α-synuclein and aggravates neurodegeneration in a *Drosophila* model of Parkinson's disease. Hum. Mol. Genet. *24*, 6675–6686.
Sztalryd, C., and Brasaemle, D.L. (2017). The perilipin family of lipid droplet proteins: Gatekeepers of intracellular lipolysis. Biochim. Biophys. Acta Mol. Cell Biol. Lipids *1862*, 1221–1232.
Thiam, A.R., Antonny, B., Wang, J., Delacotte, J., Wilfling, F., Walther, T.C., Beck, R., Rothman, J.E., and Pincet, F. (2013). COPI buds 60-nm lipid droplets from reconstituted water–phospholipid–triacylglyceride interfaces, suggesting a tension clamp function. Proc. Natl. Acad. Sci. U. S. A. *110*, 13244–13249.
Van Den Brink, D.M., Cubizolle, A., Chatelain, G., Davoust, N., Girard, V., Johansen, S., Napoletano, F., Dourlen, P., Guillou, L., Angebault-Prouteau, C., et al. (2018). Physiological and pathological roles of FATP-mediated lipid droplets in Drosophila and mice retina. PLOS Genet. *14*, e1007627.
Wang, S., Yoo, S., Kim, H.-Y., Wang, M., Zheng, C., Parkhouse, W., Krieger, C., and Harden, N. (2015). Detection of in situ protein-protein complexes at the Drosophila larval neuromuscular junction using proximity ligation assay. J. Vis. Exp. JoVE 52139.
Welte, M.A. (2015). Expanding Roles for Lipid Droplets. Curr. Biol. *25*, R470–R481.
Welte, M.A., and Gould, A.P. (2017). Lipid droplet functions beyond energy storage.

Biochim. Biophys. Acta *1862*, 1260–1272.
Welte, M.A., Gross, S.P., Postner, M., Block, S.M., and Wieschaus, E.F. (1998). Developmental Regulation of Vesicle Transport in Drosophila Embryos: Forces and Kinetics. Cell *92*, 547–557.
Xu, N., Zhang, S.O., Cole, R.A., McKinney, S.A., Guo, F., Haas, J.T., Bobba, S., Farese, R.V., and Mak, H.Y. (2012). The FATP1-DGAT2 complex facilitates lipid droplet expansion at the ER-lipid droplet interface. J. Cell Biol. *198*, 895–911.
Yan, Y., Wang, H., Hu, M., Jiang, L., Wang, Y., Liu, P., Liang, X., Liu, J., Li, C., Lindström-Battle, A., et al. (2017). HDAC6 Suppresses Age-Dependent Ectopic Fat Accumulation by Maintaining the Proteostasis of PLIN2 in Drosophila. Dev. Cell *43*, 99-111.e5.
Yasuhara, J.C., Baumann, O., and Takeyasu, K. (2000). Localization of Na/K-ATPase in developing and adult Drosophila melanogaster photoreceptors. Cell Tissue Res. *300*, 239–249.
Yu, Y.V., Li, Z., Rizzo, N.P., Einstein, J., and Welte, M.A. (2011). Targeting the motor regulator Klar to lipid droplets. BMC Cell Biol. *12*, 9.

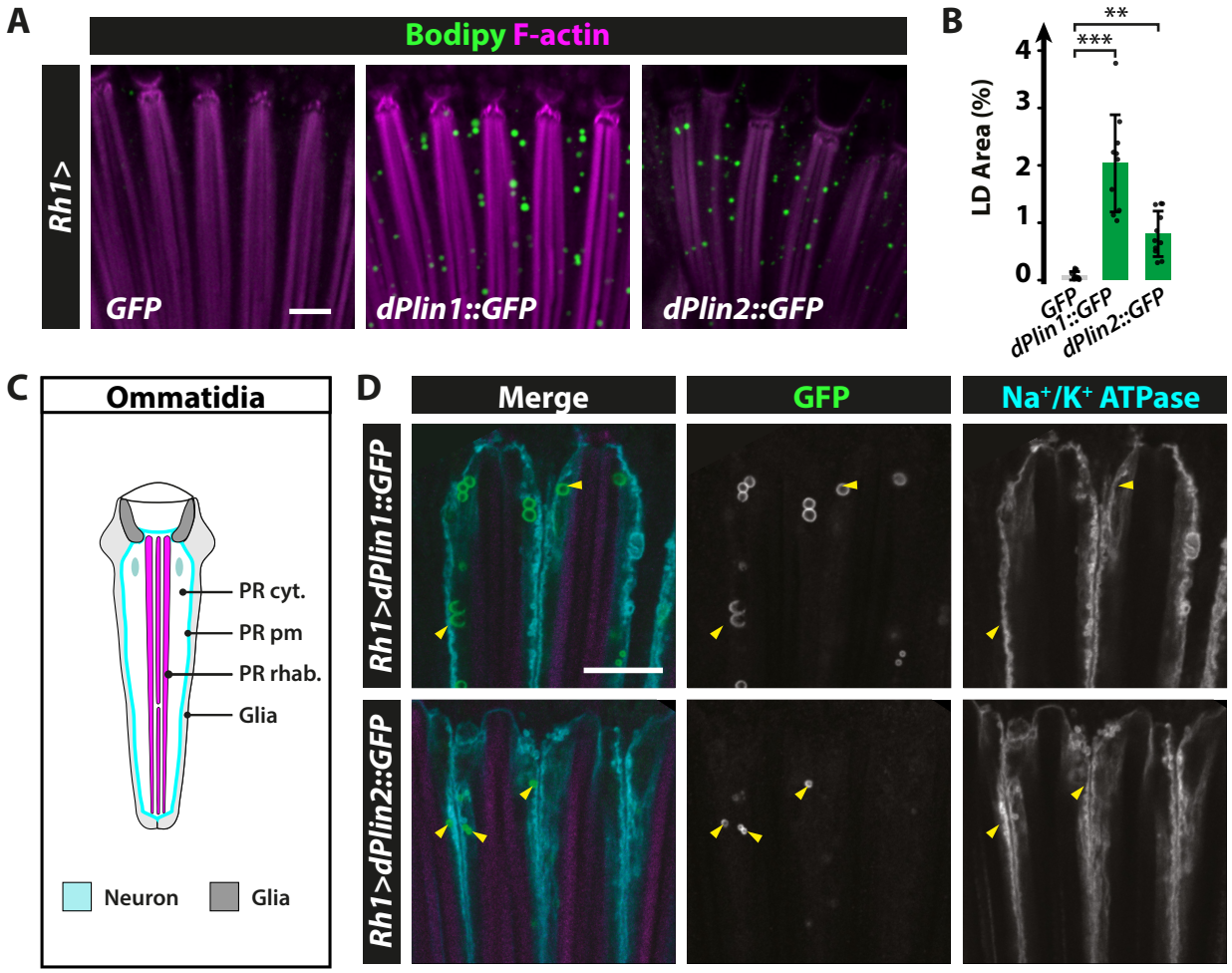

Girard et al. Figure 2

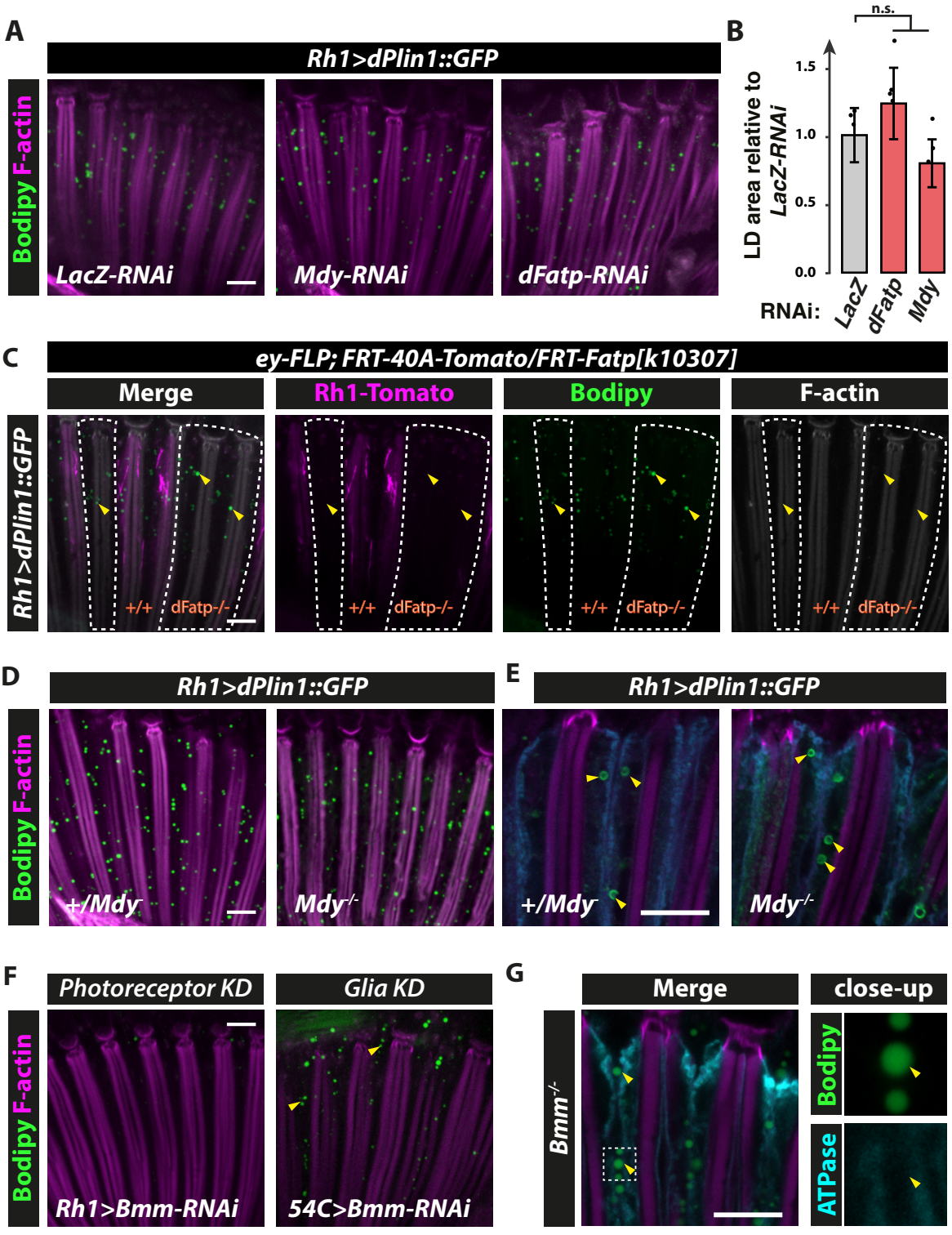

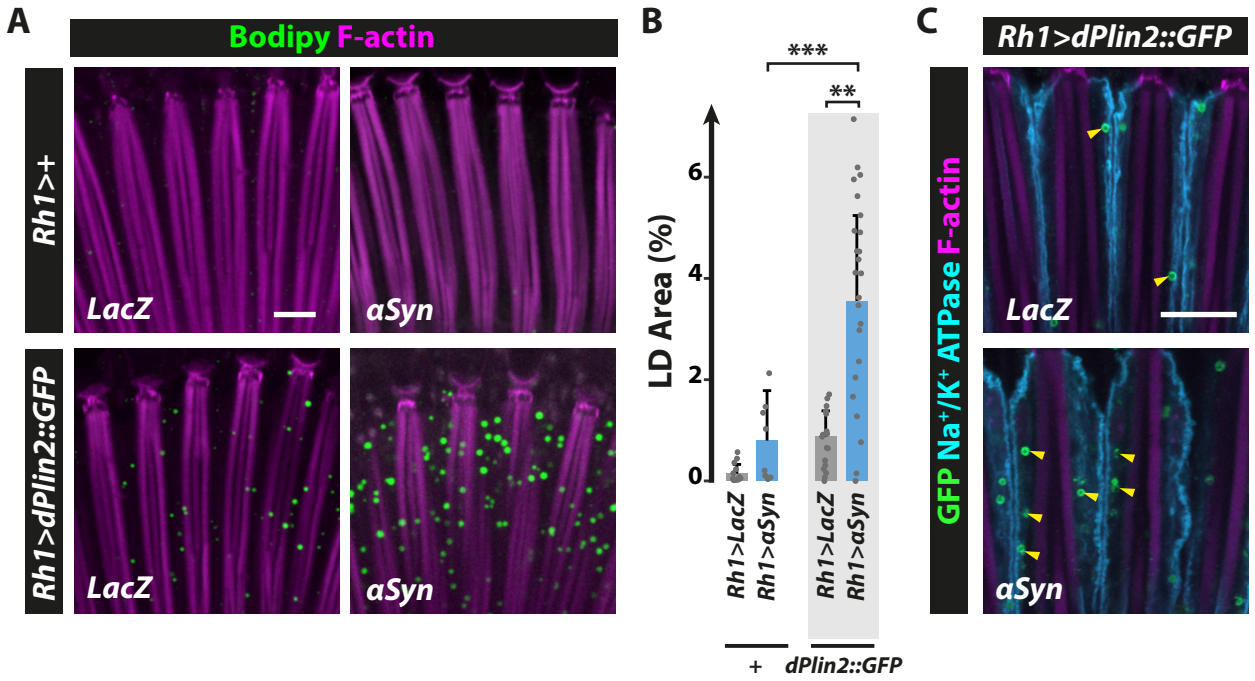

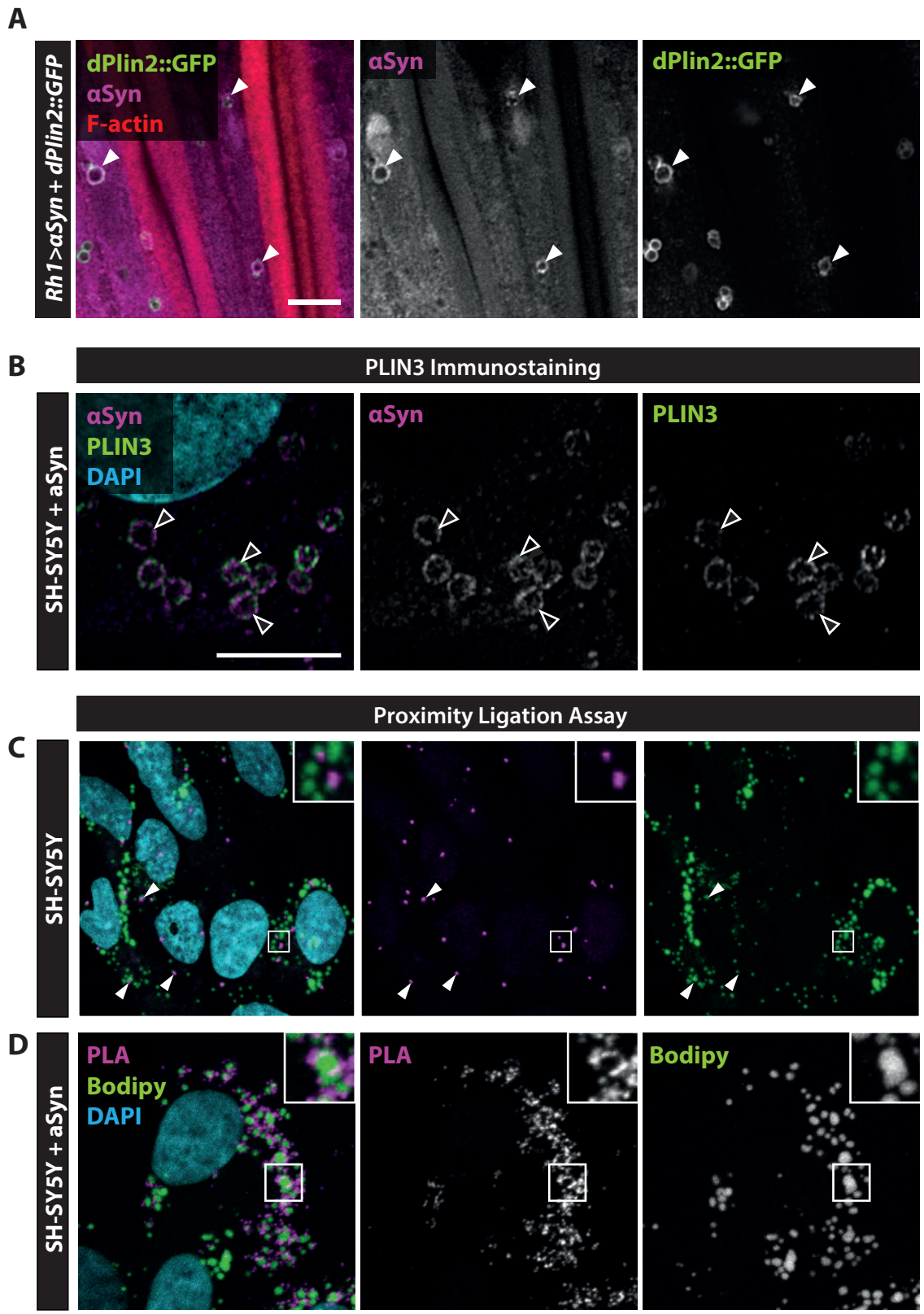

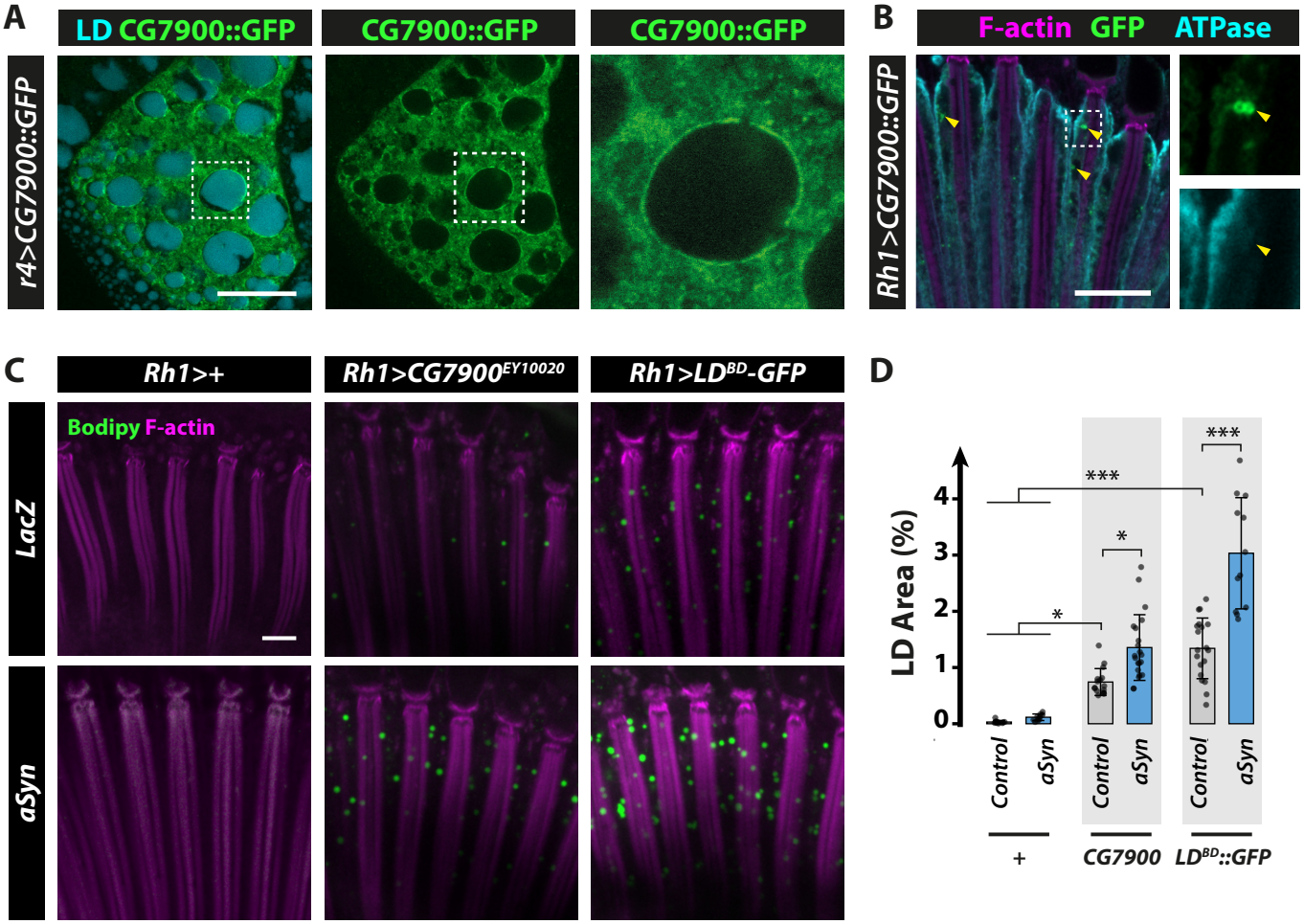

Girard et al. Figure 6

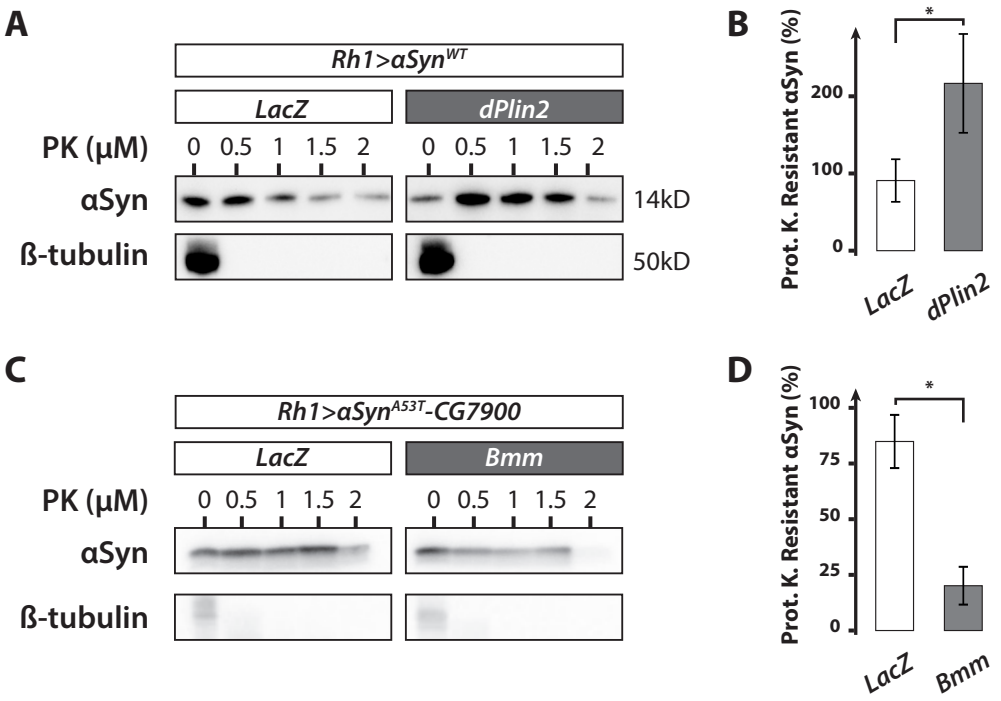

Girard et al. Figure 7

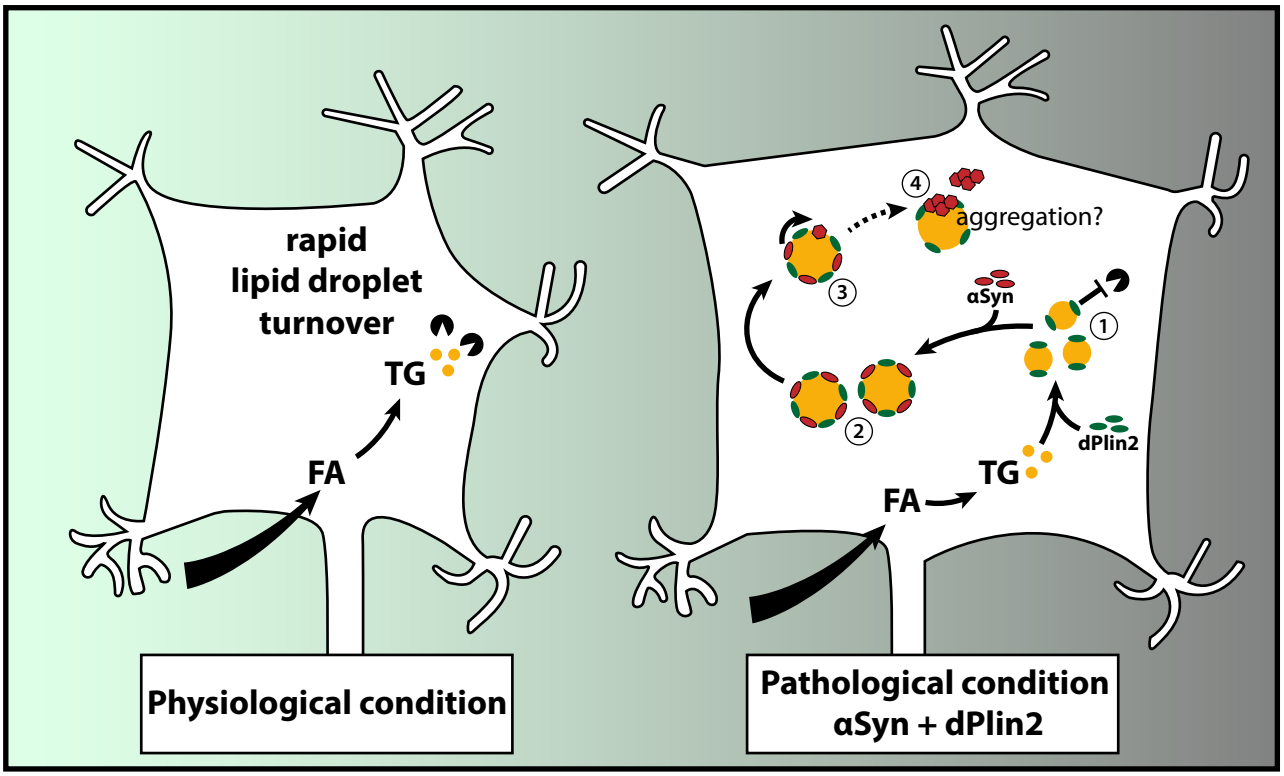

Girard et al. Figure Supplemental 1

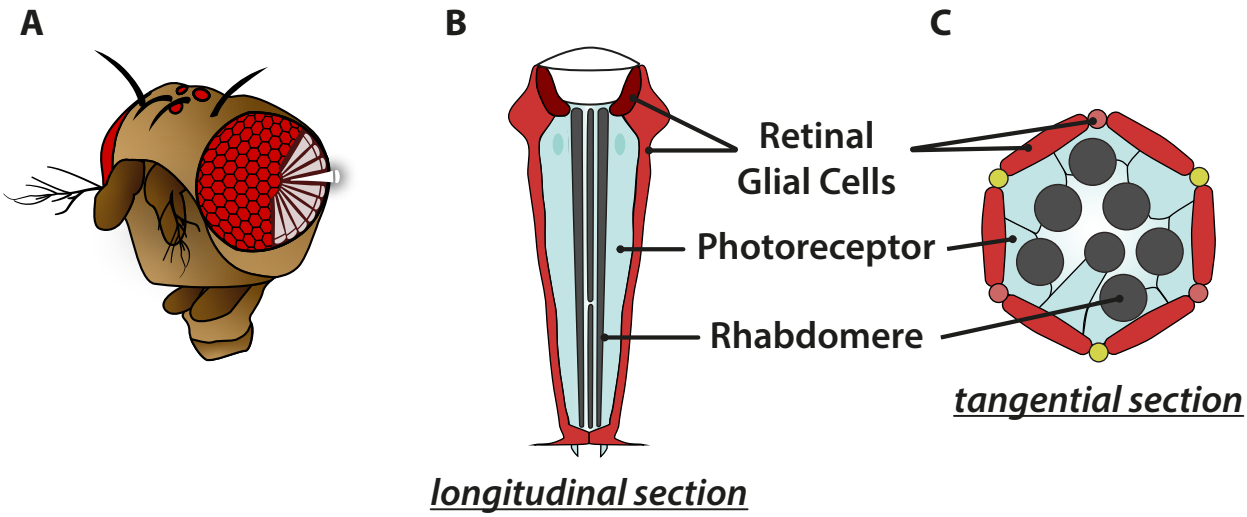

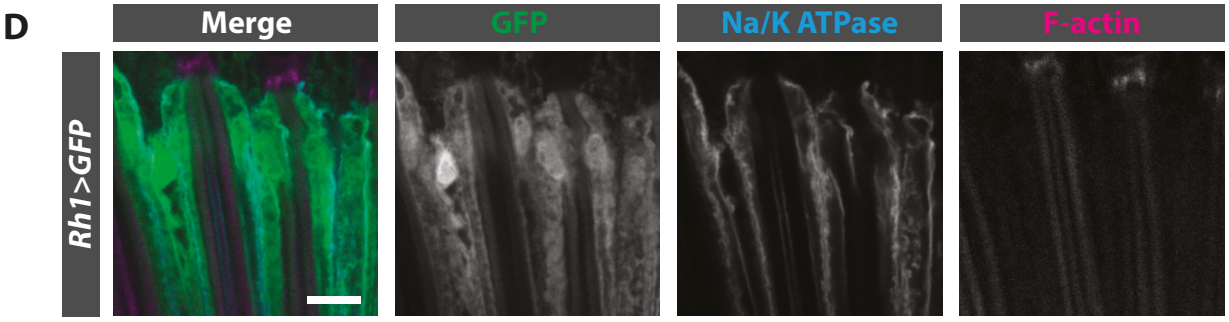

Girard et al. Figure Supplemental 2

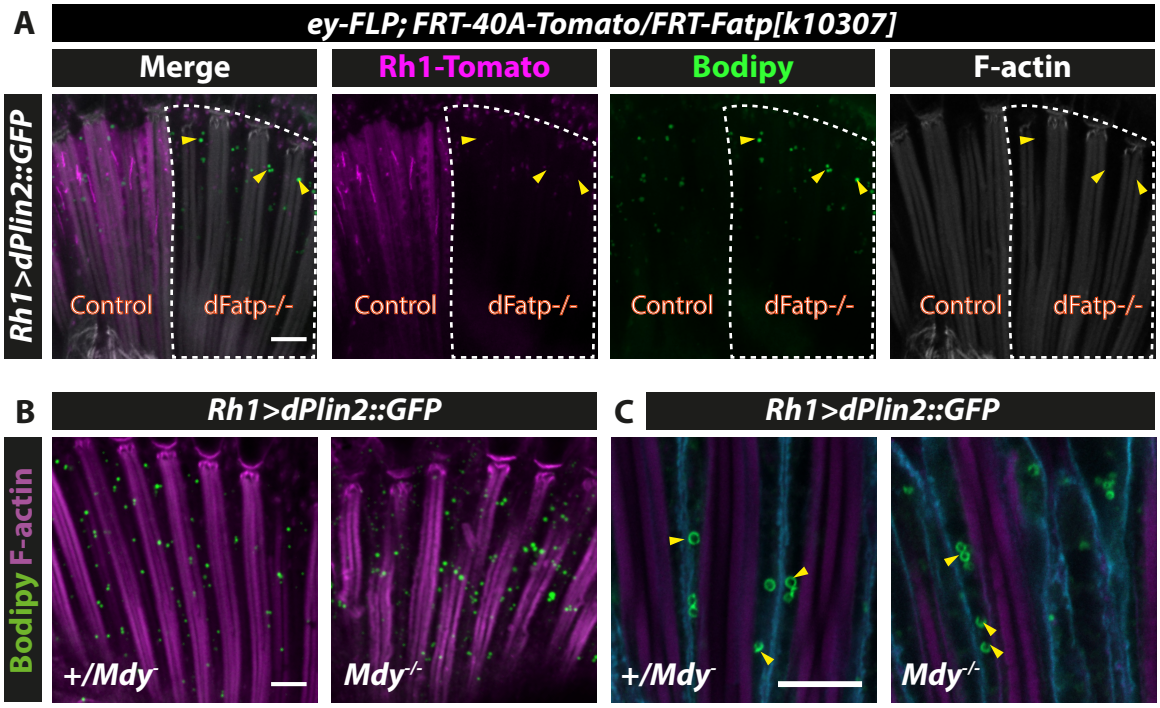

Girard et al. Figure Supplemental 3

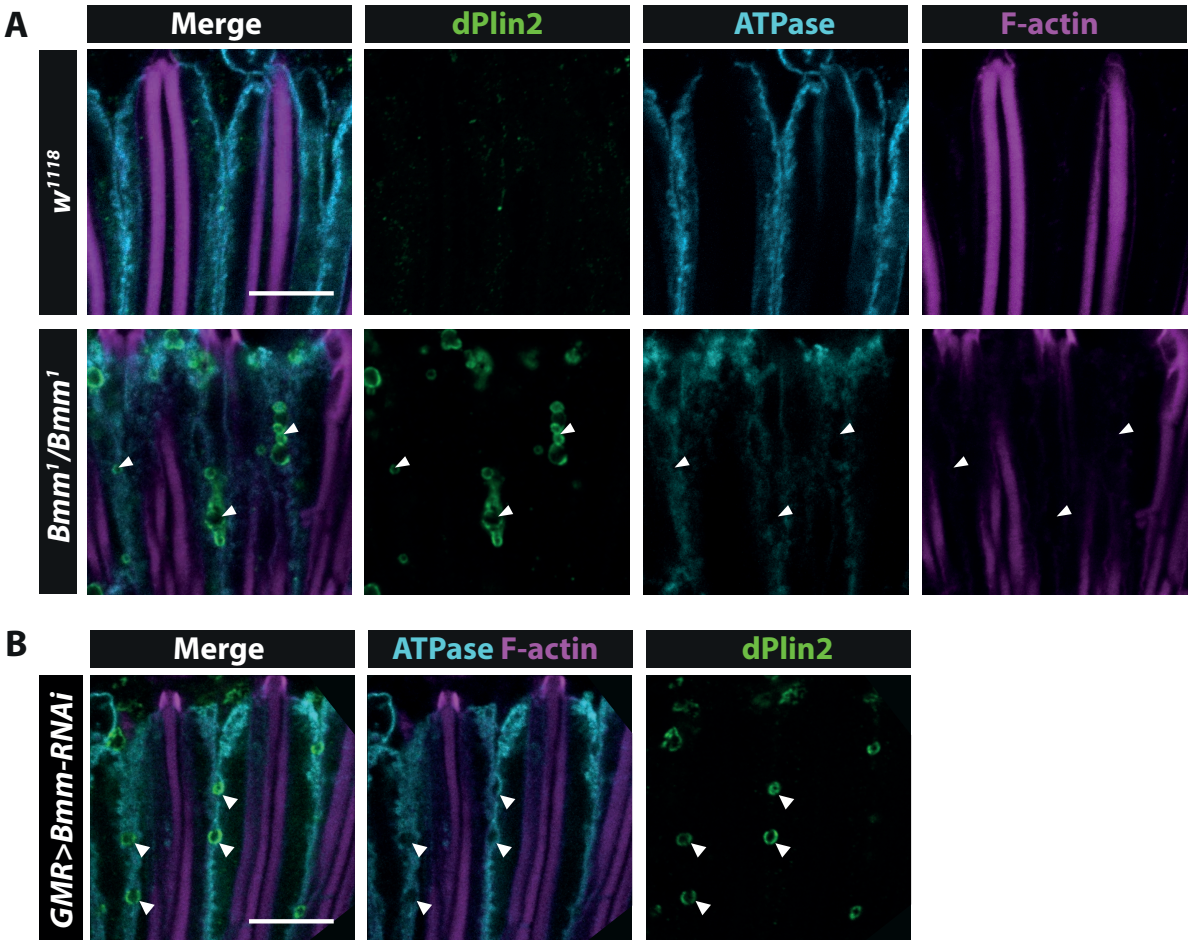

Girard et al. Figure Supplemental 4

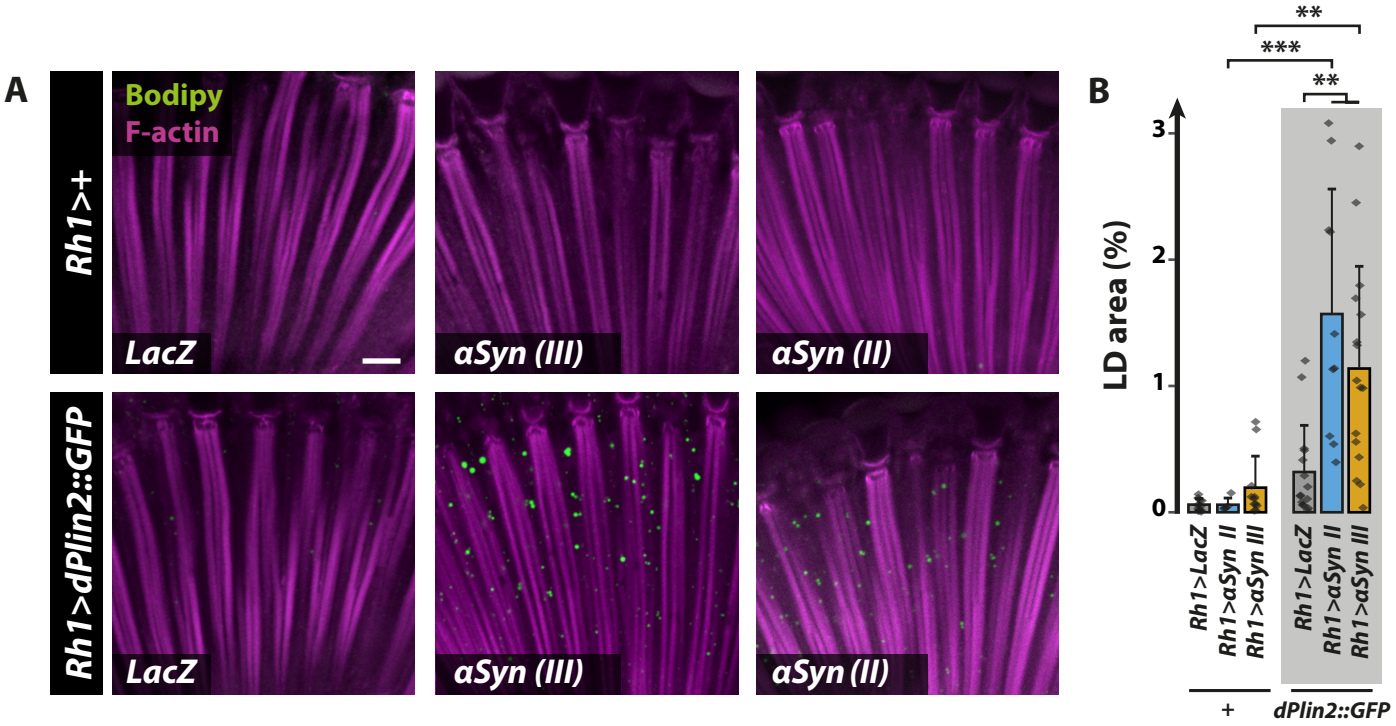

Girard et al. Figure Supplemental 5

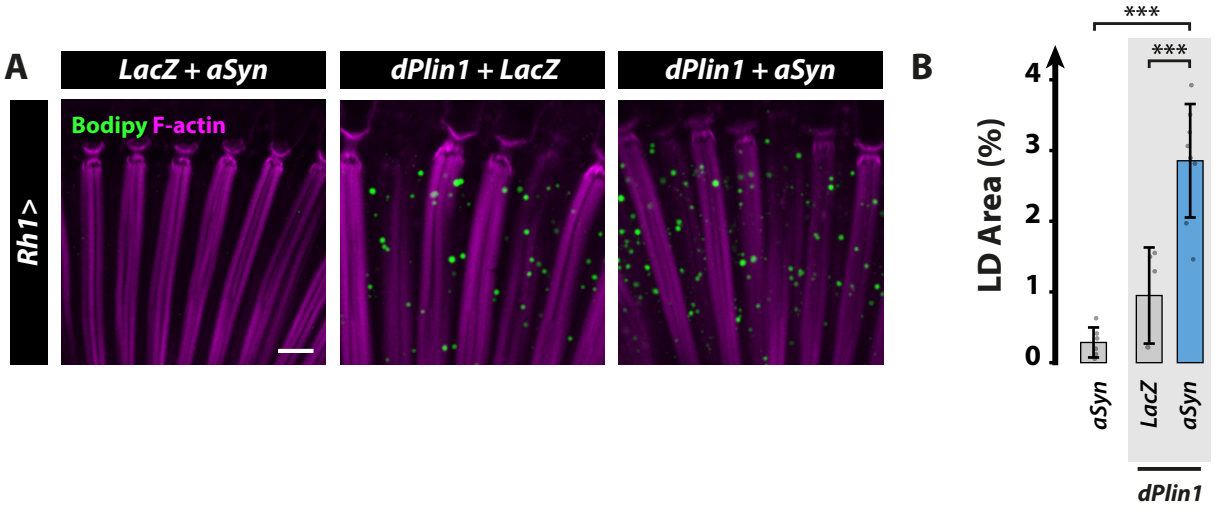

Girard et al. Figure Supplemental 6

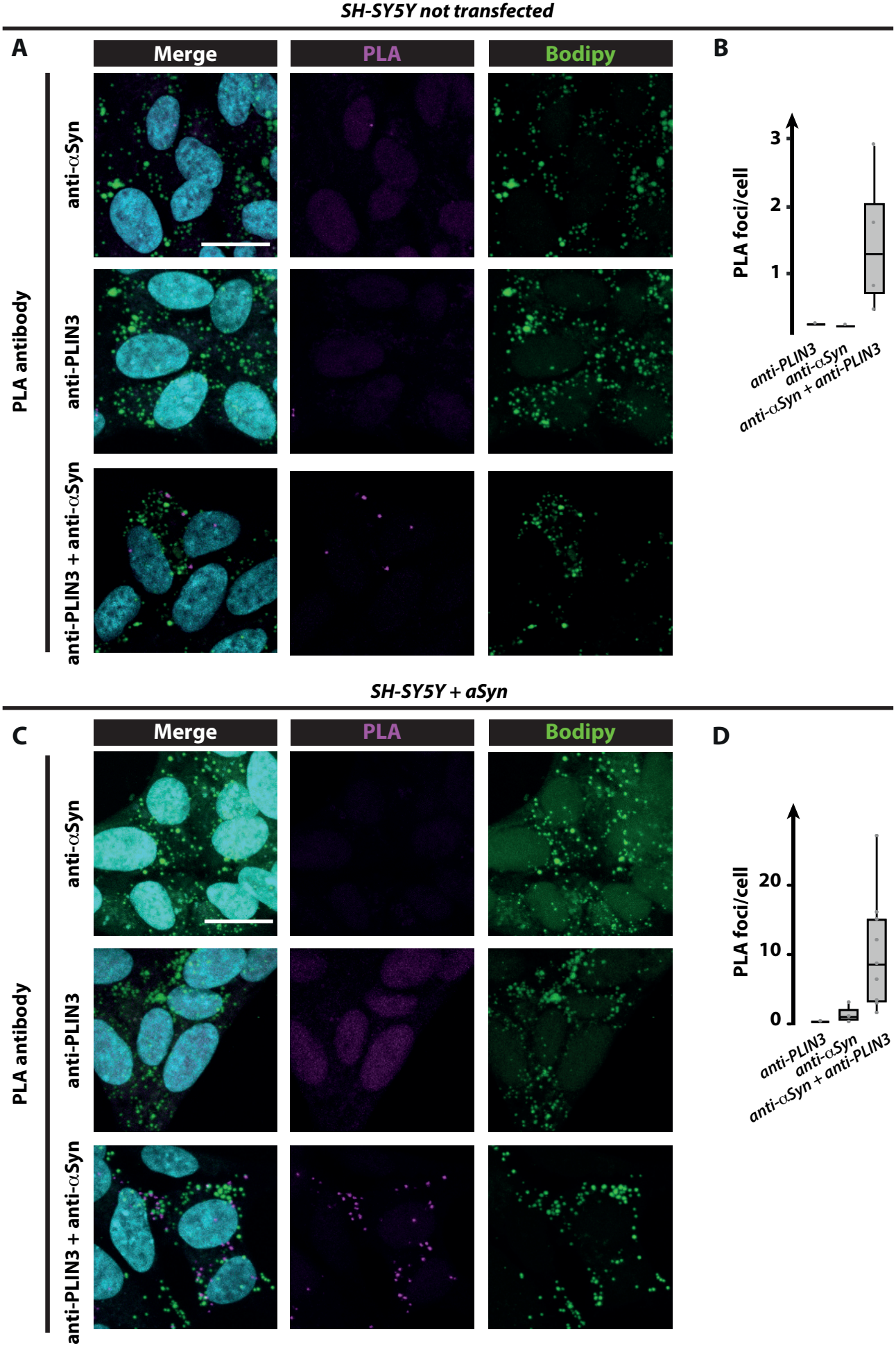

Girard et al. Figure Supplement 7

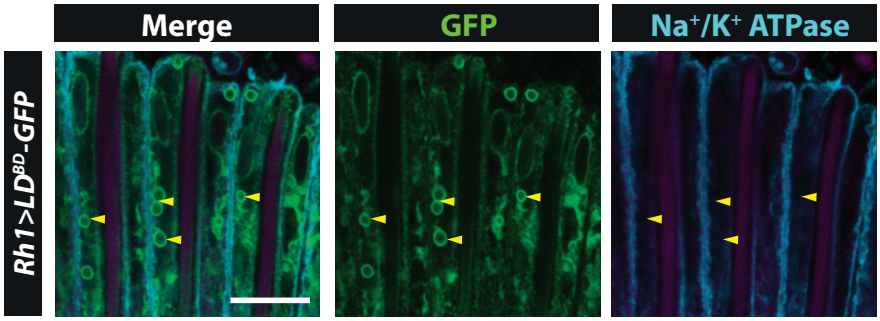

Girard et al. Figure Supplemental 8

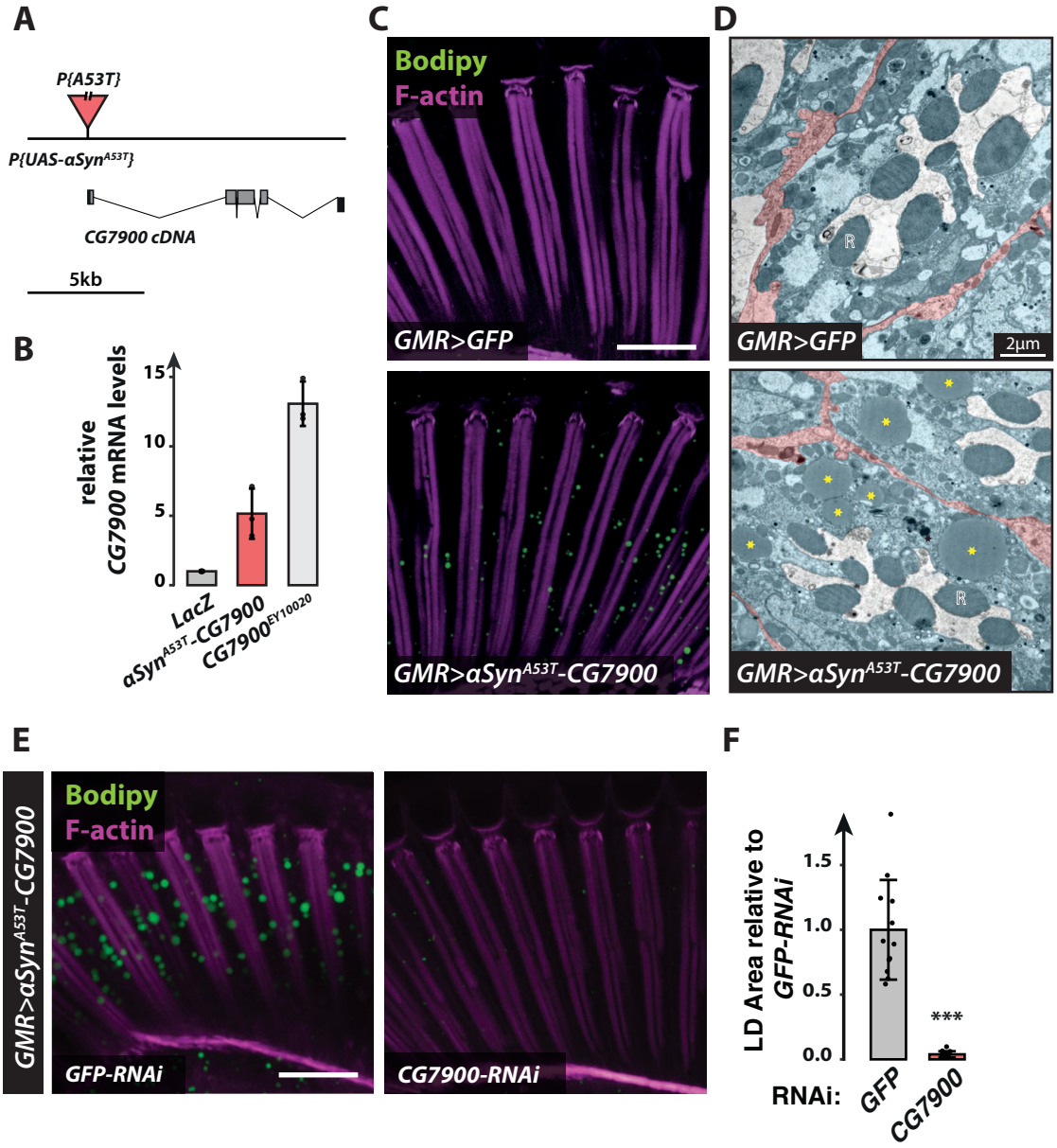

Girard et al. Figure Supplemental 9

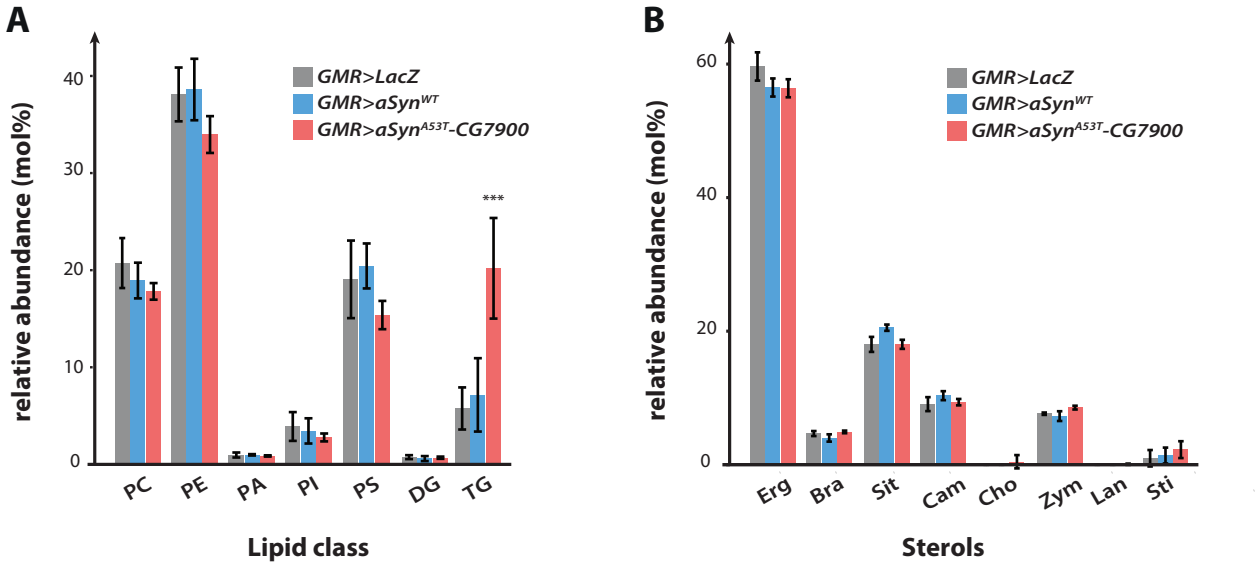

Girard et al. Figure Supplemental 10

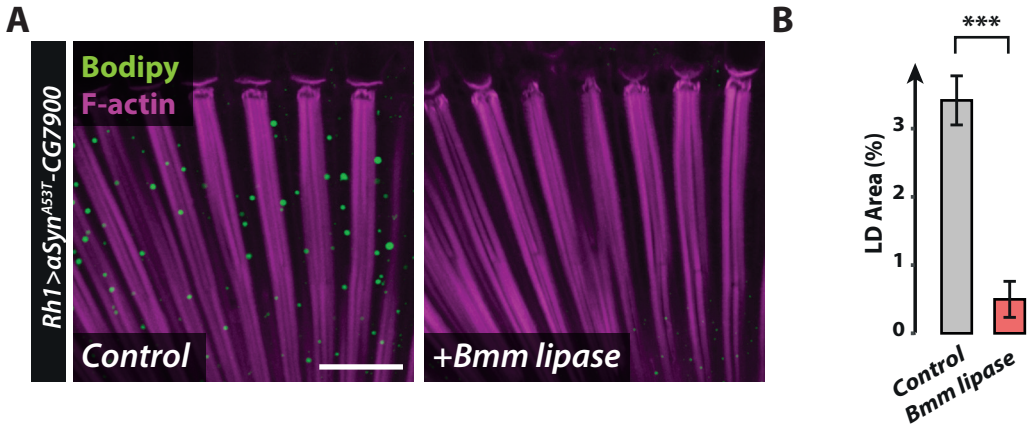

Legends of Supplemental Figures

Figure S1. The *Drosophila* retinal structure.

(A) Diagram of a *Drosophila* compound eye. The eye is composed of about 800 repeated units called ommatidia (hexagonal shapes). Longitudinal sections (shown in white) of the ommatidia allow visualization of the retinal cells that span the entire width of the retina.

(B) Diagram of a longitudinal section of one ommatidium. Each ommatidium is composed of 8 photoreceptor neurons (light blue), each containing one rhabdomere (dark gray), and glial cells (also known as primary, secondary and tertiary retinal pigment cells; maroon, medium red and, light red respectively) that are juxtaposed to photoreceptor neurons from the apical to the basal retina.

(C) Diagram of a cross-section of one ommatidium. In addition to the glial cells (2 primary, 6 secondary [medium red] and 3 tertiary [light red] pigment cells), each ommatidium contains 3 bristle cells (yellow) originating from the neuronal lineage.

(D) Immunostaining of whole-mount retinas from flies expressing GFP in photoreceptor (*Rh1-GAL4*). Photoreceptor plasma membranes are in cyan (anti-Na+/K+ ATPase) and rhabdomeres are in magenta (phalloidin-rhodamine). GFP is visible only in the photoreceptor cytoplasm. Scale bar, 10µm.

Figure S2. dPlin2-induced LDs do not require canonical enzymes involved in TG synthesis (*Fatp*, *Mdy*) in photoreceptor neurons.

(A) LD staining of whole-mount retinas from flipase mediated FRT dFatp^{k10307} mutant clone in conjunction with expression of *dPlin2::GFP* in photoreceptors (*Rh1-GAL4*). LDs are in green (Bodipy), wild type photoreceptors are in grey (*FRT40A-tdTomato^{ninaC}*) and rhabdomeres are in magenta (phalloidin-rhodamine labeling of F-actin). LDs are visible in photoreceptors lacking dFatp (mutant clone surrounded by dashed line). Scale bar, 10 µm.

(B, C) LD staining of whole-mount retinas from *mdy^{QX25}* heterozygous and homozygous flies expressing *dPlin2::GFP* in photoreceptors (*Rh1-GAL4*). Scale bar, 10 µm.**(B)** LDs are in green (Bodipy), and rhabdomeres are in magenta (phalloidin-rhodamine). **(C)** Photoreceptor plasma membranes are in cyan (anti-Na^+/K^+ ATPase) and rhabdomeres are in magenta (phalloidin-

rhodamine) dPlin2 ::GFP stains LDs as a ring shape in the photoreceptor cytoplasm (yellow arrowheads).

Figure S3. Loss of Bmm promotes LDs in glial cells but not in photoreceptor neurons.

(A) Immunostaining of whole-mount retinas from control w^{1118} or homozygous Bmm^{1} mutant flies. LDs are in green (anti-dPlin2), photoreceptor plasma membranes are in cyan (anti-Na^+/K^+ ATPase) and rhabdomeres are in magenta (phalloidin-rhodamine). Scale bar, 10 µm.

(B) Immunostaining of whole-mount retinas from flies expressing RNAi targeting *Bmm* lipase under the control of the pan-retinal driver *GMR*. LDs are visible in green (anti-dPlin2), photoreceptor plasma membranes are in cyan (anti-Na^+/K^+ ATPase) and rhabdomeres are in magenta (phalloidin-rhodamine). Scale bar, 10 µm.

Figure S4. αSyn and dPlin2 synergize to induce LD accumulation in photoreceptor neurons.

(A) LD staining of whole-mount retinas from flies with photoreceptor neuron-specific expression of *LacZ* (control) or αSyn^{WT} (two independent lines located on second and third chromosome; the line aSyn III is used elsewhere in the article) alone or in conjunction with *dPlin2::GFP*. LDs are shown in green (Bodipy) and photoreceptor rhabdomeres are shown in magenta (phalloidin-rhodamine). Scale bar, 10 µm.

(B) Quantification of LD area from the images shown in (A). Mean ± SD. ***p<0.001, **p<0.01 by ANOVA with Tukey's HSD test.

Figure S5. αSyn enhances dPlin1-induced LD accumulation in *Drosophila* photoreceptor neurons.

(A) LD staining of whole-mount retinas from flies expressing LacZ (control) or human αSyn alone or in conjunction with *dPlin1::GFP* in photoreceptor neurons (*Rh1-GAL4*). LDs are in green (Bodipy) and photoreceptor rhabdomeres are in magenta (phalloidin-rhodamine). Scale bar, 10 µm.

(B) Quantification of LD area from images shown in (A). Mean ± SD. ***p<0.001 by ANOVA with Tukey's HSD test.

Figure S6. αSyn co-localizes with PLIN3 in human neuroblastoma cells.

(A). Proximity ligation assay between αSyn and PLIN3 in non-transfected SH-SY5Y cells. The PLA signal generated by close proximity of the two protein-bound primary antibodies shown in magenta is not visible when antibody against PLIN3 or αSyn are used separately. LDs are in green (Bodipy), and nuclei are counterstained with DAPI (cyan). Scale bars, 15 µm.

(B). Quantification of the number of PLA foci per cell seen in (A).

(C). Proximity ligation assay between αSyn and PLIN3 in transfected SH-SY5Y cells with αSyn^{WT}. The PLA signal generated by close proximity of the two protein-bound primary antibodies shown in magenta is not visible when antibody against PLIN3 or αSyn are used separately. LDs are in green (Bodipy), and nuclei are counterstained with DAPI (cyan). Scale bars, 15 µm.

(D). Quantification of the number of PLA foci per cell seen in (C).

Figure S7. The expression of GFP-tagged lipid-binding domain of Klarsicht induces LD accumulation in photoreceptor neurons.

Immunostaining of whole-mount retinas from flies with photoreceptor neuron-specific expression of the minimal lipid-binding domain of Klarsicht fused to GFP (*UAS-LD^{BD}-GFP*) (Yu et al., 2011). GFP localizes to the ring-shaped structures (yellow arrowheads) located between photoreceptor plasma membranes in cyan (anti-Na^+/K^+ ATPase) and rhabdomere in magenta (phalloidin-rhodamine). Scale bar, 10 µm.

Figure S8. Characterization of the *P{UAS-αSyn^{A53T}}CG7900* transgenic line promoting LD accumulation in photoreceptors

(A) Diagram of the genomic localization of the *P{UAS-αSyn^{A53T}}* transgene mapped using the Splinkerette protocol. The P-element carrying the upstream activating sequence (UAS) upstream of the coding sequence of human *αSyn^{A53T}* is inserted in the promoter region of *CG7900*.

(B) RT-qPCR analysis of *CG7900* mRNA in heads of flies expressing *LacZ, αSyn^{A53T}-CG7900,* or *CG7900* (EP-[UAS] insertion, EY10020) under the control of the pan-retinal driver *GMR-GAL4*. mRNA levels are expressed as the mean ± SD of triplicates relative to the level in control (*GMR>LacZ*) flies.

(C) LD staining of whole-mount retinas from flies with pan-retinal expression of *GFP* or *αSyn^{A53T}-CG7900*. LDs are shown in green (Bodipy) and photoreceptor rhabdomeres are in magenta (phalloidin-rhodamine). Scale bar, 20 µm.

(D) TEM images of ommatidia cross-sections from 60-day-old flies with pan-retinal expression of *GFP* (top panel) or *αSyn^{A53T}-CG7900* (bottom panel). Each panel shows a representative cross-section of one ommatidium containing seven photoreceptors (false-colored blue) with central rhabdomeres (R) surrounded by retinal glial cells (false-colored orange). Yellow asterisks indicate LDs accumulating in the photoreceptor cytoplasm of flies expressing *αSyn^{A53T}-CG7900*. Scale bar, 2 µm.

(E) LD staining of whole-mount retinas from flies expressing *αSyn^{A53T}-CG7900* in conjunction with GFP-RNAi or CG7900-RNAi in photoreceptors (*Rh1-GAL4*). LDs are shown in green (Bodipy) and photoreceptor rhabdomeres are in magenta (phalloidin-rhodamine). Scale bar, 20 µm.

(F) Quantification of LD area from the images shown in (E). Mean ± SD. ***p<0.001 by t-test.

Figure S9. Expression of αSyn^{A53T}-CG7900 induces TG accumulation in *Drosophila* retina.

(A) Main lipid classes detected by shotgun mass spectrometric analysis of retinas from 20-day-old flies with pan-retinal expression of *LacZ* (control, gray bars), *αSyn^{WT}* (blue bars), or *αSyn^{A53T}-CG7900* (red bars). Lipid quantities are expressed as mole % within each species. Data show the mean ± SD of five biological replicates. Expression of *αSyn^{A53T}-CG7900* induces a significant accumulation of triacylglycerols (TG) in *Drosophila* retina. PC, phosphatidylcholine; PE, phosphatidylethanolamine; PA, phosphatidic acid; PI, phosphatidylinositol; PS, phosphatidyl serine; DG, diacylglycerol.

(B) Sterol composition of retinas from 20-day-old_flies with pan-retinal expression of LacZ (control, gray bars), *αSyn^{WT}* (blue bars), or *αSyn^{A53T}-CG7900* (red bars). Lipid quantities are expressed as mole % within each species. Data show the mean ± SD of 5 biological replicates. Erg, ergosterol; Bra, brassicasterol; Sit, sitosterol; Cam, campesterol; Cho, cholesterol; Zym, zymosterol; Lan, lanosterol and Sti, stigmasterol

Figure S10. Bmm promotes the degradation of αSyn^{A53T}-CG7900 induced-LDs in *Drosophila* photoreceptors

(A) LD staining of whole-mount retinas from flies expressing *αSyn^{A53T}-CG7900* alone or in conjunction with Bmm lipase in photoreceptors (*Rh1-GAL4*). LDs are shown in green (Bodipy) and photoreceptor rhabdomeres are in magenta (phalloidin-rhodamine). Scale bar, 20 μm.

(B) Quantification of LD area from the images shown in (E). Mean ± SD. ***p<0.001 by t-test.